



UNIVERSITY OF LEEDS

This is a repository copy of *A combined scheme for maximising the output power of a Photovoltaic array under partial shading conditions*.

White Rose Research Online URL for this paper:

<https://eprints.whiterose.ac.uk/181780/>

Version: Accepted Version

Article:

Etarhouni, M orcid.org/0000-0003-1626-2585, Chong, B and Zhang, L (2022) A combined scheme for maximising the output power of a Photovoltaic array under partial shading conditions. *Sustainable Energy Technologies and Assessments*, 50. 101878. ISSN 2213-1388

<https://doi.org/10.1016/j.seta.2021.101878>

© 2021, Elsevier. This manuscript version is made available under the CC-BY-NC-ND 4.0 license <http://creativecommons.org/licenses/by-nc-nd/4.0/>.

Reuse

This article is distributed under the terms of the Creative Commons Attribution-NonCommercial-NoDerivs (CC BY-NC-ND) licence. This licence only allows you to download this work and share it with others as long as you credit the authors, but you can't change the article in any way or use it commercially. More information and the full terms of the licence here: <https://creativecommons.org/licenses/>

Takedown

If you consider content in White Rose Research Online to be in breach of UK law, please notify us by emailing eprints@whiterose.ac.uk including the URL of the record and the reason for the withdrawal request.



eprints@whiterose.ac.uk
<https://eprints.whiterose.ac.uk/>

A Combined Scheme for Maximising the Output Power of a Photovoltaic Array under Partial Shading Conditions

Mohamed Etarhouni, Benjamin Chong, Li Zhang
School of Electrical and Electronic Engineering, University of Leeds
Woodhouse lane, Leeds, LS2 9JT, UK

*Correspondence: Tarhouni_88@yahoo.com / fy09mse@leeds.ac.uk; Tel: +447597037004

Abstract:

The power generation performance of a solar array can be enhanced by using a scheme that combines various techniques, including Maximum Power Point Tracking (MPPT), a PV array reconfiguration, and DC-DC converters for current and voltage matching. This paper presents a novel combination of three techniques and a closed-loop control strategy to improve the performance of a large PV array initially in Tied-Cross-Ties (TCT) interconnection. Firstly a modified Magic Square-Enhanced Configuration (MS-EC) is used to permute the module positions in the array. The chosen example is a 6×6 TCT array. The resultant arrangement is then divided into four 3×3 TCT sub-arrays. Irradiance Equalisation (IE) is applied to each sub-array to make the irradiation levels match approximately between its rows. Finally, a Series-Parallel Differential Power Processing (SP-DPPs) converter scheme is applied to the four sub-arrays for maximum power point tracking. Experimental tests are presented to validate the transfer function models of these converters and the designed control scheme. The combined scheme performance is evaluated under static and dynamic shading patterns; it compares favourably with a TCT array using only bypass diodes by showing an average power gain of **11-48%** and an efficiency of **98.95%**.

Keywords: Magic Square-Enhanced Configuration (MS-EC), Irradiance Equalisation (IE), Differential Power Processing (DPP) converters, Maximum power generation, TCT

Nomenclature:

<i>Abbreviation</i>		
BCC	Bidirectional Cuk Converter	V_{TCT2} Voltage of the sub-TCT ₂ array
BL	Bridge Linked	V_{TCT3} Voltage of the sub-TCT ₃ array
DC	Direct Current	V_{TCT4} Voltage of the sub-TCT ₄ array
DPP	Differential Power Processing	I_{TCT1} Current of the sub-TCT ₁ array
GMPP	Global Maximum Power Point	I_{TCT2} Current of the sub-TCT ₂ array
		I_{TCT3} Current of the sub-TCT ₃ array

HC	Honey-Comb	I_{TCT4}	Current of the sub-TCT ₄ array
IBC	Inverted-Buck Converter	P_{T1}	Total power of BCC-unit 1
INC	Incremental Conductance	P_{T2}	Total power of BCC-unit 2
IE	Irradiance Equalisation	K_{11}	Duty ratio of BCC ₁
I-V	Current-Voltage	I_{T1}	Total current of BCC-unit 1
ML	Mismatched Power Loss	I_{T2}	Total current of BCC-unit 2
MPP	Maximum Power Point	V_{T1}	Total voltage of BCC-unit 1
MS	Magic Square	V_{T2}	Total voltage of BCC-unit 1
MS-EC	Magic Square-Enhanced Configuration	I_{L1}	The current flowing in L_1
P	Parallel	k	The total number of modules
P-V	Power-Voltage	Δv_o	Output voltage ripples
P&O	Perturb & Observe	Δi_L	Inductor current ripples
P+I	Proportional and Integral	R_{PV1}	Resistor of PV ₁ module
PSC	Partial Shading Condition	R_{PV2}	Resistor of PV ₁ module
PV	Photovoltaic	F_S	Switching Frequency
S	Series	F_C	Cut-off Frequency
STC	Standard Testing Condition	K_{DPP}	Duty ratio of the DPP
TCT	Tied-Cross-Ties	V_{FE}	Voltage of the Front-End
<i>Symbols</i>		V_{DPP}	Output voltage of the DPP
i	row number	K_{FE}	Duty ratio of the Front-End
j	column number		
p	PV module number		
N_{SW}	Number of switches		
N_{PV}	Number of PV modules		
V_{TCT1}	Voltage of the sub-TCT ₁ array		

1. Introduction

Partial Shading Condition (PSC) can result in hotspot formation, power loss and mismatched load within modules of a PV array [1-4]. Installed PV arrays are generally shadowed by nearby buildings, cloud coverage, bird droppings and dust [1]. Bypass diodes are traditionally connected across sub-chains within a PV array to alleviate the problem. This often

leads to multiple peaks in the Power-Voltage (P-V) characteristic curve and a reduction in generated power below what is theoretically possible [2].

To mitigate the partial shading effect on a PV array, one method is to interconnect the PV modules in different ways, forming different array configurations [5]. Conventional configurations include **Series (S)**, **Parallel (P)**, **Tied-Cross-Ties (TCT)**, **Bridge-Linked (BL)**, and **Honey-Comb (HC)**. Variety of new connections were proposed in recent years [6], and their performances under partial shading has been compared [7-11]. Series and parallel arrays are the poorest choices due to their low output current and voltage, respectively. The TCT array is found to have the most overall resilience to shading. Its crossties minimise the possibility of turning on bypass diodes under several shading patterns and can increase the lifetime of the PV array [7, 9]. Thus, apart from the interconnection practicalities, the only drawback of the TCT array can be the extra cabling costs of the crossties, these also being nearly redundant under uniform illumination. Other promising techniques for mitigating the limitations of the TCT structure have been proposed, these are based on reconfiguration strategies [3, 5, 12-18]. The reconfiguration methods are classified as dynamic or static.

Various dynamic reconfiguration methods based on the Irradiance Equalisation (IE) principle are available in the literature [16, 19-21]. The earliest [21] focused on the simplest reconfiguration IE technique to minimise partial shading losses in the PV array system. Another proposed IE algorithm [19] determines the sums of solar irradiances of the PV array rows for all possible array arrangements, and the one with the best equalisation index is chosen. These earlier IE methods are impractical for large PV arrays due to requiring excessive computational time and a very large number of sensors. The proposed version of the irradiance equalisation method in [16] can alleviate these limitations. This is a static reconfiguration of a simple TCT array which is modified or “reconfigured” by conceptually moving any module to a different physical location in the array, without changing any electrical connections. The well-known examples of physical relocation algorithms are the improved SuDoKu [22], Magic Square (MS) [23], Odd-Even [24], Futoshiki [25] and Competence Square (CS) [4]. The number of iterations required by these algorithms can be cumbersome for larger array size, and they can fail MPPT under specific shading patterns. The demerits of these static techniques are overcome by the Magic-Square Enhanced Configuration (MS-EC) [26].

Power Electronic Equalisers including the Module Integrated Converters MICs [27], series and parallel schemes of Differential Power Processing DPP converters [28-31] are altogether

used at the sub-module level to achieve a true MPP tracking and enhance the total array system efficiency. However, these techniques can still add losses to the system and increase the size and cost. Various MPP tracking methods have been developed and further enhanced in the literature. For instance, the well-known MPP tracking methods [33-35], such as perturb & observe (P&O) and incremental conductance (INC), have been widely adopted due to their satisfactory tracking efficiency performance and simplicity of installation under uniform irradiation conditions. The work in [36] also used a hybrid technique combining analytical and differential evolution algorithms based on an accurate two-diode PV model to extract the maximum power available under non-uniform irradiation conditions. However, these techniques may fail to track the global peak point (i.e., highest power peak on the P-V curve), as they get trapped into the local power peak under changing irradiation conditions. In addition, evolutionary MPP tracking algorithms, such as Genetic Algorithm (GA) [37], Particle Swarm Optimisation (PSO) [38] and Flower Pollination Algorithm (FPA) [39], can be time-consuming and lead to high fluctuations when searching for the maximum power under PSCs.

The main objective of this paper is to enhance the power generation performance of a solar PV array under partial shading conditions. This can be achieved by using a scheme that combines various techniques, including an efficient maximum power point tracking scheme, a PV array reconfiguration technique, and DC-DC converters for current and voltage matching processing.

This paper proposes a novel combined scheme to improve the power generation performance of a large PV array, originally in Tied-Cross-Ties (TCT) interconnection, operating under partial shading conditions. The scheme is intended to be used for large-scale PV applications, such as the solar farms. Three different techniques are combined; these are the Magic-Square Enhanced Configuration (MS-EC) modified from that of [26], Irradiance Equalisation (IE) and Series and parallel Differential Power Processing (DPP). The approach offers the following advantageous features which are not seen by the previously published work: 1) able to obtain the best light dispersing effect, due to using MS-EC to physically rearrange the modules in a TCT array corresponding to shading patterns. 2) By using IE, proper matching of solar irradiation levels between rows of the PV array can be obtained hence reducing multiple power peaks. 3) Giving accurate and good dynamic performance maximum power extraction by controlling series and parallel converters under all possible partial shading conditions. This combined scheme also gives the advantage of reducing the number of required converters for MPP control compared to the system shown in [27]; hence suppressing power

losses. Moreover the paper presents an advanced model predictive control algorithm for MPP tracking using DPP power processing. The method applies a PV single-diode model compared to that in [36], to predict the MPP voltage values under PSCs which are then fed as the reference values to the P+I controller used. The parameters of the P+I controllers are optimised based on the transfer functions of the DPP converters. Experimental tests are presented to validate the transfer function models of these converters and the designed control system. The performance of this combined scheme is evaluated under various static and dynamic shading conditions and compares favourably with the traditional TCT array scheme using only bypass diodes and the other existing reconfigurations techniques.

The paper is organised as follows: Section 2 describes in detail the proposed combined scheme. The control scheme and its experimental verifications for the whole PV-converter system are discussed in Section 3. Finally, Section 4 presents the simulation studies validating the power performance of the new scheme and its comparison with other well-known techniques.

2. A Combined Scheme for Optimizing the Power Performance of a PV Array

As described above, none of the existing reconfiguration techniques, such as MS-EC and IE, can alone extract the highest possible power of a PV array system under most shading patterns. This is due to the limitations discussed for each reconfiguration technique. The paper offers a novel combined scheme, as shown in Fig. 1 that can overcome the limitations of the former reconfiguration techniques; hence the maximum power generation under various shading conditions is possible.

2.1. Overview of the scheme

This combined scheme is applied to a 6x6 TCT array under non-uniform irradiation conditions. Firstly, a modified MS-EC static reconfiguration algorithm is used to rearrange the TCT array in Fig. 1(a) by shuffling 36 modules into four TCT square sub-groups where each group consists of 9 modules arranged into a 3x3 TCT array as shown in Fig. 1(b). Hence, the modified version of MS-EC in this paper can be applied to either symmetrical or asymmetrical PV arrays to achieve the best light dispersing effect, unlike the one proposed previously in [26], where only odd square arrays are considered.

The next step involves applying IE electrical reconfiguration algorithm shown in Fig. 1(c). The aim is to equalise the solar intensity levels over the rows and columns of the individual four TCT squares for more power extraction. This should ideally decrease the multiple power peaks which occur due to unequal solar irradiance within the rows in each sub-group.

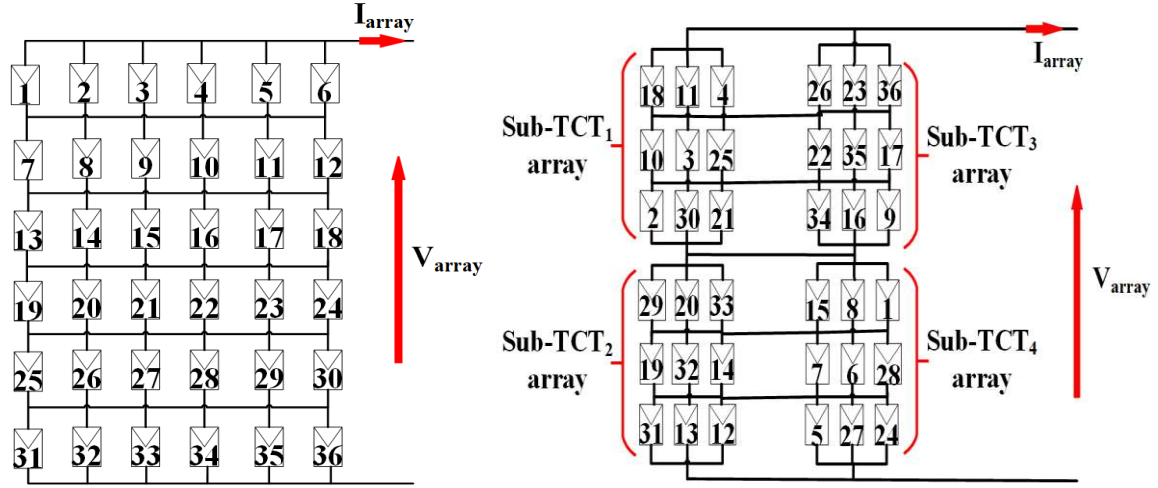
Finally, the Series-Parallel Differential Power Processing converter scheme is applied here by using Bidirectional Ćuk Converter (BCC) to link each Sub-TCT array pairs in a string, two such strings (i.e. TCT₁ & TCT₂ for BCC₁, TCT₃ & TCT₄ for BCC₂) are formed, as can be seen in Fig. 1(c). These parallel strings are linked to a DC-bus by connecting DPPs in series with each string. The benefit of using BCCs here is that the current flowing into each TCT array sub-group is independent of each other when partial shading occurs. Thus, the total current of the array is increased compared to that of the TCT array structure in Fig. 1(a), where no DPPs or reconfiguration algorithms are used. The use of parallel DPP converters based on the Inverted Buck Converter (IBC) structure ensures voltage equalization over each string.

2.2. Methodology for implementing the combined scheme technique in the PV array system

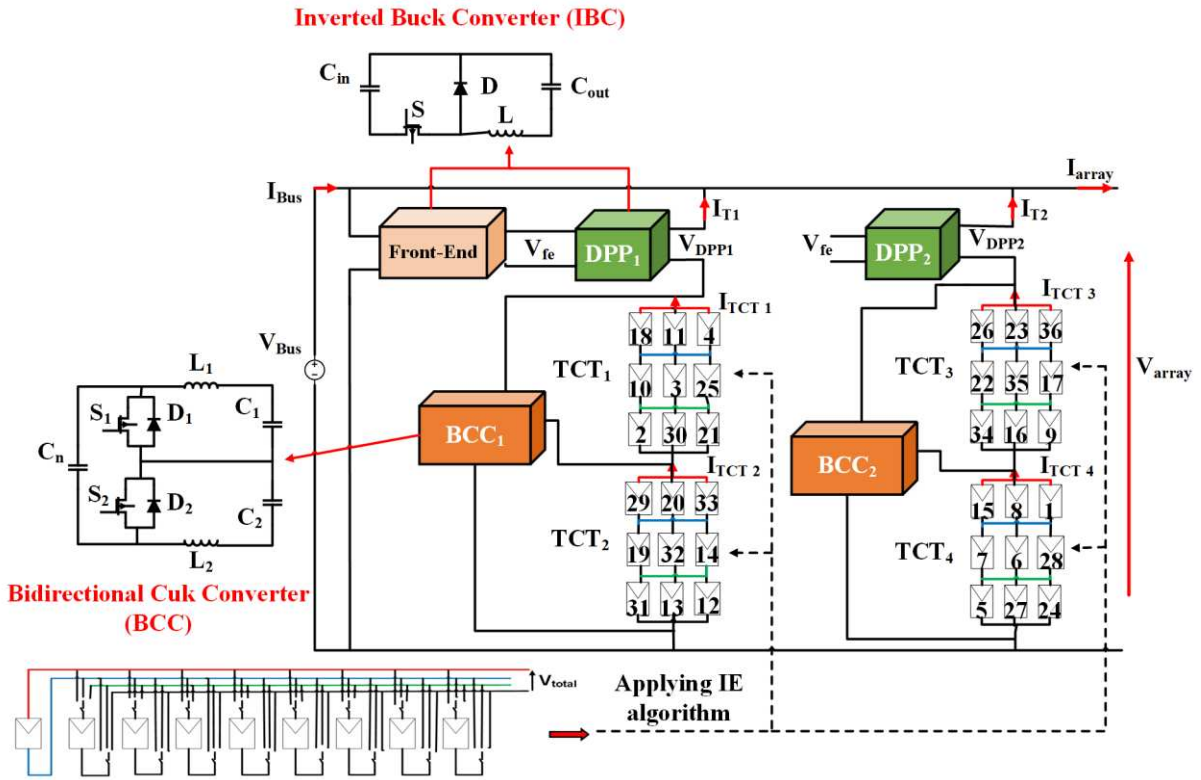
The overall flowchart in Fig. 2(a) illustrates the complete procedure of implementing the combined scheme for a chosen example of 6×6 TCT array interconnection. The methodology procedure is detailed and summarised as follows:

Step 1: An MS algorithm improved from that described in [26] is used to rearrange the example 6×6 array leading to an enhanced configuration MS-EC. It is assumed that the shading occurs in a group of adjacent modules. The algorithm aims to move all these PV modules into different areas within the array. The underlying aim of this procedure is that the sum of the current in one row of the array limits the current in other rows, which are connected in series with it. Hence, the current reduction caused by shading should be maximally spread among the rows.

The initial structure of the 6×6 PV array is shown in Fig. 3(a). It is clearly seen that each module is assigned to its corresponding cell; hence, all modules are sequentially ordered with a reference number (i.e., 1, 2, 3...36). The physical location of each module is indicated by the row and column numbers I, j respectively, which are placed at the left and top sides of the array table in Fig. 3(b). The PV module 5, for instance, is located at position coordinate of (0, 4) before reconfiguration where $i_5 = 0$ and $j_5 = 4$.



(a) An example of a 6x6 TCT array structure (b) Applying the MS-EC method to reconfigure TCT array and dividing it into sub-array groups



(c) The combined scheme using the three techniques (MS-EC + DPP converters + IE) to extract the maximum power available from a shaded Photovoltaic (PV) array

Fig. 1. The full implementation process of the combined PV array scheme based on an example of a 6x6 TCT array structure

- The full implementation steps of the MS-EC algorithm are illustrated in Figs. 3(b)-(f) and in the flowchart shown in Fig. 2(b). This algorithm begins by finding the new PV module 1 (PV_1) location based on its new evaluated coordinates expressed by $i_{1,new} =$

$\text{int} \left\lfloor \frac{n}{2} \right\rfloor$, and $j_{1,\text{new}} = n - 1$, where $n = \sqrt{k} = 6$. Hence, this module is moved to (3, 5). According to Fig. 3(c), the new location of each module is determined by the position of the immediately preceding module. The new coordinate of the next module p is, for example, obtained by $i_{p,\text{new}} = i_{p-1} - 1$ and $j_{p,\text{new}} = j_{p-1} + 1$. However, when either $i_{p,\text{new}}$ or $j_{p,\text{new}}$ becomes higher than 5 or less than 0, the new location is updated according to the following conditions:

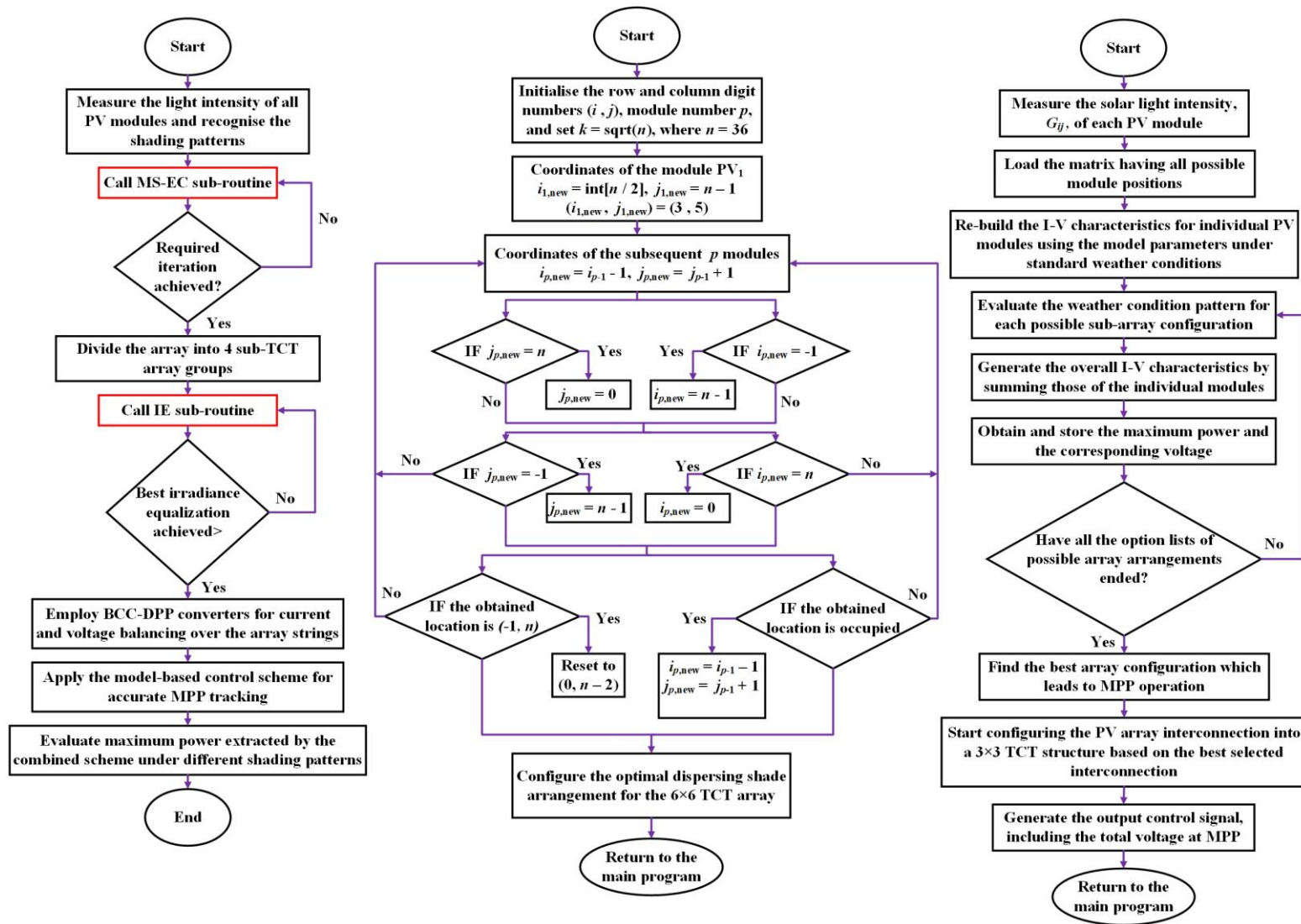
1. If $j_{p,\text{new}} = n$, then reset it to $j_{p,\text{new}} = 0$; **else if** $j_{p,\text{new}} = -1$, then $i_{p,\text{new}} = n - 1$. For example, PV module 2's new location first becomes (3 -1, 5 +1) = (2, 6) which is reset to (2, 0) and moves back into the square. Two other conditions need to be trapped;
2. If the obtained location is occupied, therefore, the new coordinates are updated by:

$$i_{p,\text{new}} = i_{p,\text{new}} + 1, \quad j_{p,\text{new}} = j_{p,\text{new}} - 2$$

3. If the determined position is at (-1, n), then reset the new location coordinate to (0, $n - 2$).
4. If $i_{p,\text{new}} = -1$, then reset it to $i_{p,\text{new}} = n - 1$; **else if** $i_{p,\text{new}} = n$, then $i_{p,\text{new}} = 0$.

- The new arrangement for this 6×6 array after using the above-explained shuffling algorithm technique is shown in Fig. 3(c). Note, Fig. 3(f) shows the division of the array into four sub-TCT square groups.

Step 2: Although the shading spread is now well-distributed over the array after applying the MS-EC algorithm, direct application of BCC-DPPs converters structure to the sub-divided array groups may not be appropriate. This is due to that some of the sub-array groups may experience multiple power peaks due to the inequality of the solar irradiance within their rows. Therefore, the IE approach is used to reduce the number of power peaks so that searching for global MPP for this system can be more straightforward and accurate.



(a) Main program flowchart of the combined scheme

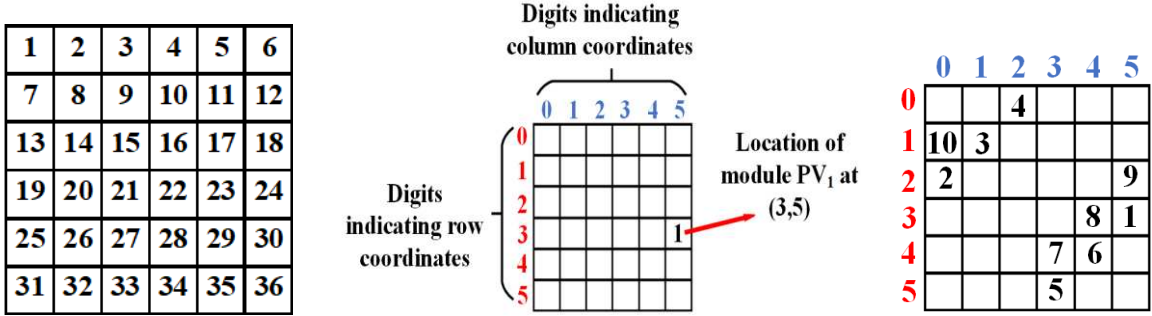
(b) MS-EC algorithm sub-routine flowchart

(c) IE algorithm sub-routine flowchart

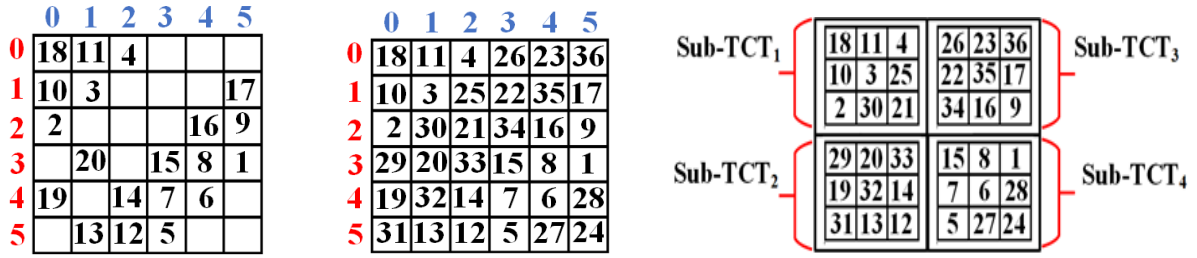
Fig. 2. A complete flowchart of the combined technique procedure for a 6x6 TCT array structure

- The IE method uses a sophisticated switching scheme to overcome the issue of irradiance inequality between the rows and reduce the current limiting effect caused by PSCs. For each sub-group, the PV modules are connected intelligently into a tied-cross-ties configuration through switches as seen in Fig. 1(c); hence, the system can balance the effective irradiance across each tier (i.e. row) in the TCT structure. Each sub-TCT group requires $N_{SW} = 2 N_{PV}$ number of switches, where N_{SW} refers to a single-pole m-throw type while N_{PV} is the number of PV modules, leading to a total of 64 active switching devices used for the IE reconfiguration process.
- The principles of the proposed IE algorithm are illustrated in the flowchart shown in Fig. 2(c), where the S-function is programmed via MATLAB-SIMULINK tool environment. This function has nine inputs where each refers to its solar irradiance level; thus, the output should give a reference MPP voltage of a particular TCT square group after being optimally reconfigured. Hence, this reference PV voltage is then fed to the closed-loop controller scheme, as discussed in the following section.

Step 3: For accurate MPP tracking of the whole PV array system, BCC-DPPs converters can offer further power control flexibility to all sub-TCT arrays. In this system, two Bidirectional Ćuk Converters are used, as shown in Fig. 1(c), each cross-connecting two chain-lined 3x3 sub-array groups (i.e., TCT₁ & TCT₂ for BCC₁, and TCT₃ & TCT₄ for BCC₂) forming two TCT-BCC units. A DPP converter is then wired in series with each of these two TCT-BCC units, and the whole chain is connected to the DC bus; many such chains can be connected in parallel to the DC line, though there are only two in this work, as shown in Fig. 1(c). It is required to adjust both sub-array currents and string voltages, which is realised here by this system using BCCs for current balancing and DPPs for voltage balancing. The converter topologies are the Front-End converter, and both DPPs (i.e., DPP₁ & DPP₂) are the Inverted Buck Converters (IBC); this scheme was discussed in detail in [28, 29]. The operating principles of these converters for a single series array string are summarised as follows:



(a) Original Structure of 6x6 TCT array (b) Allocating the first module using MS-EC (c) Reconfiguring the subsequent modules



(d) Relocating the remaining modules (e) Complete MS-EC array arrangement (f) Dividing the MS-EC structure into sub-arrays

Fig. 3. Illustration of the implementation procedure of the MS-EC algorithm for 6x6 TCT array structure

- The outer parallel-connected DPPs can regulate the summed voltage of the two serially connected TCT array units, as shown in Fig. 4 (i.e., $V_{T1} = V_{TCT1} + V_{TCT2}$ and $V_{T2} = V_{TCT3} + V_{TCT4}$), to achieve the total MPP voltage value. The ratio and sum of the two TCT voltages set their absolute values. Therefore, the output power supplied to the relative terminal DPP converter is evaluated as

$$P_{T1} = V_{T1}I_{T1} = (V_{TCT1} + V_{TCT2})I_{T1} = V_{TCT1}I_{T1} + V_{TCT2}I_{T1} \quad (1)$$

- When both TCT array units receive different illumination levels, for instance, when the TCT₂ unit is shaded, the power output generated by TCT₁ would be greater than that from TCT₂. By activating the switch pair S_1 - D_2 , as shown in Fig. 4(a), i.e., operating the converter at a fixed duty ratio K_{11} and switching frequency, the converter can bypass the excess power from TCT₁ away from passing through TCT₂. The voltages across TCT₁ and TCT₂ for the BCC₁ are related by $V_{TCT2} = V_{TCT1} \left(\frac{K_{11}}{1-K_{11}} \right)$.
- Hence, the current bypassing to the converter is expressed as:

$$I_{L1} = (I_{T1} - I_{TCT2}) \left(\frac{K_{11}}{1 - K_{11}} \right) \quad (2)$$

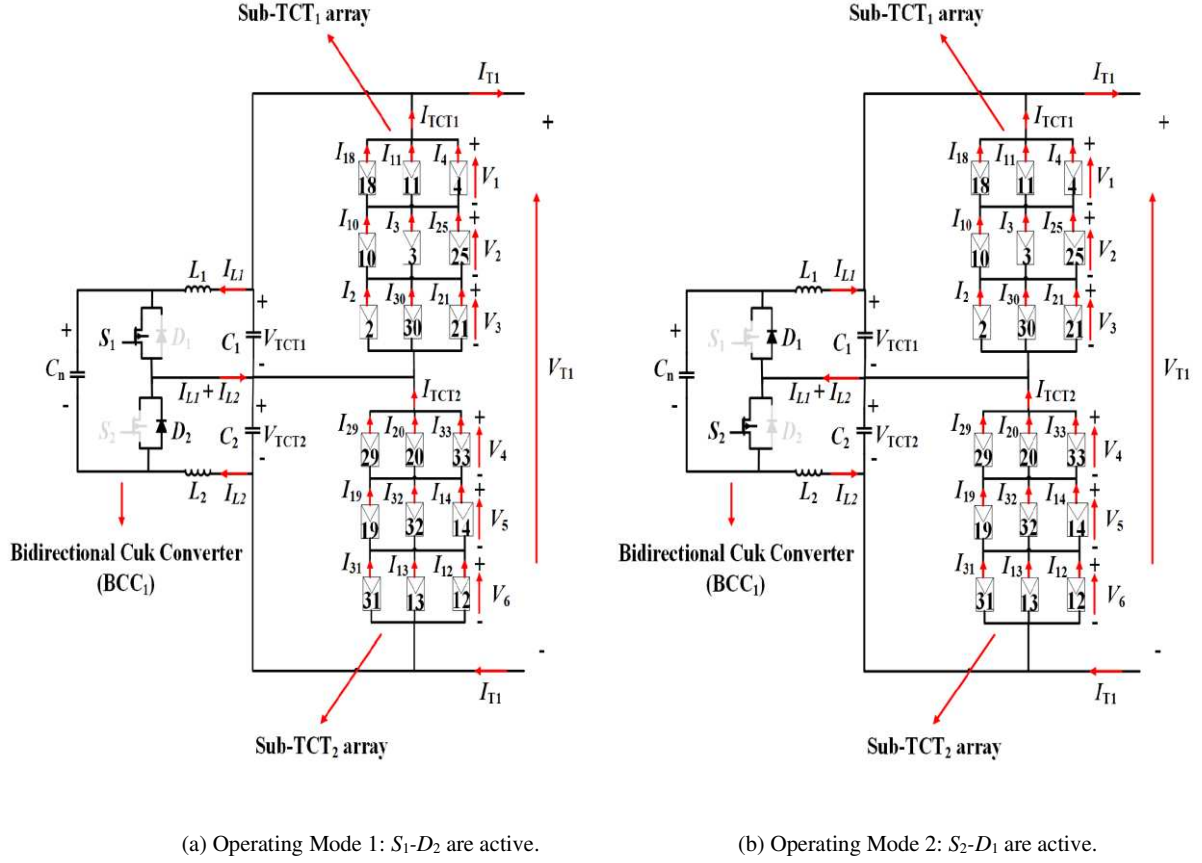


Fig. 4. Switching operating states of one Bidirectional Cuk Converter integrated with two solar sub-TCT array units

where, I_{TCT2} is the current flowing in TCT₂ sub-array group, K_{11} is the duty cycle ratios for switches S_1 ; hence, the other switch S_2 is complementary to S_1 such that $K_{21} = 1 - K_{11}$, as seen in Fig. 4(b).

- Therefore, the terminal current of the BCC_1 is now:

$$I_{T1} = I_{TCT1} - (I_{T1} - I_{TCT2}) \left(\frac{K_{11}}{1 - K_{11}} \right) = I_{TCT1}(1 - K_{11}) + I_{TCT2}K_{11} \quad (3)$$

- Thus, the total power output to the load (i.e. DPP₁) without taking losses into account is written as:

$$P_{T1} = V_{T1}I_{T1} = \left(V_{TCT1} + V_{TCT1} \left(\frac{K_{11}}{1 - K_{11}} \right) \right) (I_{TCT1}(1 - K_{11}) + I_{TCT2}K_{11})$$

$$= V_{TCT1}I_{TCT1} + V_{TCT1} \left(\frac{K_{11}}{1 - K_{11}} \right) I_{TCT2} \quad (4)$$

- This analysis indicates that the maximum power generation can still be achieved by varying the duty ratio K_{11} in (4). Hence, the shaded sub-TCT₂ can be adjusted; in other words, sub-TCT₂ can still produce power even though it is shaded.

3. Model-Based Control for the Combined Scheme in the PV Array System

A complete closed-loop control scheme is applied to the entire system with 4 TCT square arrays already reconfigured by the MS-EC and IE algorithms. The aim is to enable all TCT square PV units in parallel strings within the system shown in Fig. 1(c) to achieve their respective MPP operation under any weather conditions. Fig. 5 shows the complete combined array scheme system, which comprises two inner BCCs and two outer DPPs, including a Front-End converter. The schematic of its control scheme is also illustrated, which has two voltage controllers for the inner BCCs and terminal voltage controllers for the two DPPs.

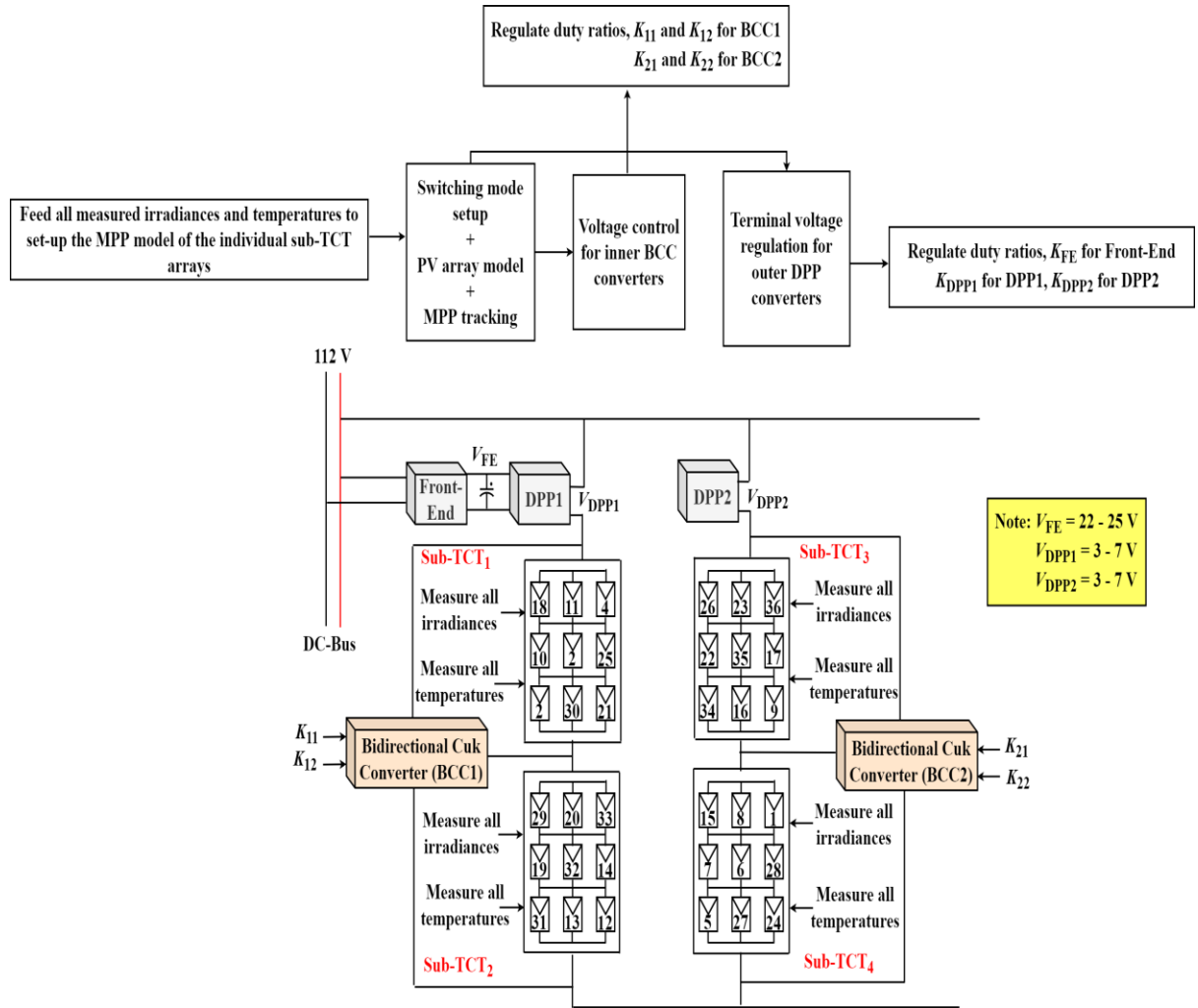


Fig. 5. A complete closed-loop control scheme for the proposed combined array structure

3.1. MPP Tracking Control for the Sub-TCT groups

Based on the measured shading conditions and sunlight levels in each TCT-square unit, the switching operating modes can first be determined according to the scheme described in Sub-section 2.2. Then, the duty ratios of the corresponding switch pairs in the inner BCCs can subsequently be determined according to the control scheme describe below.

The P+I controllers are used to determine the duty ratios of the two inner BCCs in Fig. 5. For the condition when illumination level on the sub-TCT₁ group is high than sub-TCT₂ group, the P+I controller formula determines K_{11} as:

$$K_{11} = K_{P1} \times [(V_{TCT2}^* - V_{TCT2}^m) - (V_{TCT1}^* - V_{TCT1}^m)] + K_{I1} \times [(V_{TCT2}^* - V_{TCT2}^m) - (V_{TCT1}^* - V_{TCT1}^m)], \quad (5)$$

and the duty ratio K_{21} for the complementary switch is given as

$$K_{21} = 1 - K_{11} . \quad (6)$$

Likewise, duty ratios for the BCC₂ switches are given as

$$K_{22} = K_{P2} \times [(V_{TCT4}^* - V_{TCT4}^m) - (V_{TCT3}^* - V_{TCT3}^m)] + K_{I2} \times [(V_{TCT4}^* - V_{TCT4}^m) - (V_{TCT3}^* - V_{TCT3}^m)] \quad (7)$$

$$K_{12} = 1 - K_{22} \quad (8)$$

where V_{TCT1}^m to V_{TCT4}^m are the measured PV voltages across each sub-TCT square array unit, as seen in Fig. 5, and V_{TCT1}^* to V_{TCT4}^* are their corresponding reference values, which are set using the IE procedure described by the flowchart in Fig. 2(c).

The proportional and integral gains of the P+I controllers, K_{P1} , K_{P2} and K_{I1} , K_{I2} , need to be set carefully. They are tuned based on the transfer functions for each TCT-BCC unit, as shown in Fig. 4. For example, the first transfer function that relates the small-signal terminal voltage across the TCT₁ array, ($\hat{v}_{TCT1}(s)$), to the small-signal duty ratio, $\hat{k}_{11}(s)$, expressed as:

$$G_1(s) = \frac{\hat{v}_{TCT1}(s)}{\hat{k}_{11}(s)} = - \frac{\alpha_3 s^3 + \alpha_2 s^2 + \alpha_1 s + \alpha_0}{\beta_5 s^5 + \beta_4 s^4 + \beta_3 s^3 + \beta_2 s^2 + \beta_1 s + \beta_0} V_{T1} \quad (9)$$

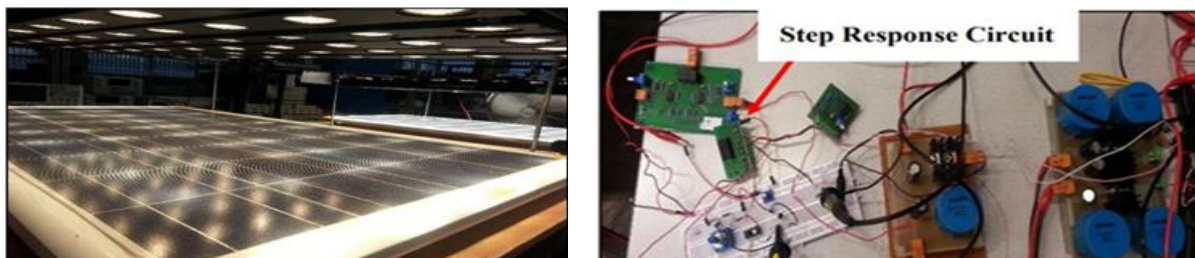
The second transfer function relates the small-signal terminal voltage $\hat{v}_{TCT2}(s)$ across TCT₂ array, and the small-signal duty ratio $\hat{k}_{11}(s)$, and given as:

$$G_2(s) = \frac{\hat{v}_{TCT2}(s)}{\hat{k}_{11}(s)} = \frac{\Omega_3 s^3 + \Omega_2 s^2 + \Omega_1 s + \Omega_0}{\beta_5 s^5 + \beta_4 s^4 + \beta_3 s^3 + \beta_2 s^2 + \beta_1 s + \beta_0} V_{T1} \quad (10)$$

Note, V_{T1} in the above transfer functions is the terminal voltage of the whole string determined by summing the voltages of the two sub-TCT groups within BCC_1 . The definitions of parameters $\beta_1, \beta_2 \dots \beta_5, \alpha_1 \dots \alpha_3, \Omega_1 \dots$ and Ω_3 , are listed in the Appendix A₁.

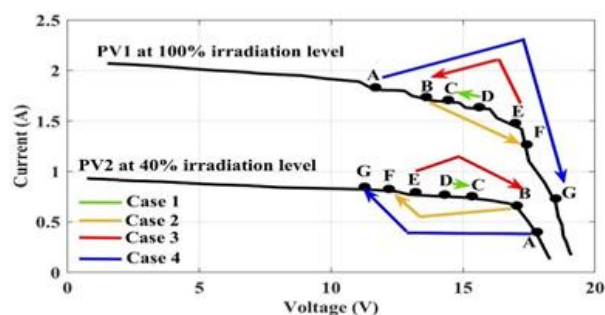
3.1.1 Experimental Validation of The BCC Mathematical Model

The verifications of the derived transfer functions for one BCC unit in Equations (9) and (10), respectively, have been carried out using a practical PV module set-up consisting of two identical SunseiSE-6000 PV modules connected on the two terminals of a BCC. Figs. 6(a) and (b) present a pair of PV modules bypassed by a Ćuk converter circuit under two controllable and identical sunlight simulators. The light intensity level for each sun-simulator can be adjusted from zero to its maximum limit (i.e., 0 to 100%), which is equivalent to a solar irradiance of about 505 W/m^2 . A single practical module can generate up to 50.05 W during shaded, i.e., standard operation condition (STC). The parameter values of the experimental PV modules and BCC are listed in Table 1. Inductors L_1 and L_2 are filtering components to eliminate the inrush current during switching either S_1 or S_2 on or off; thus, charging or discharging C_n . The frequency of the inrush current is sufficiently high so that inductor values need to be small. Note, the energy storage element C_n is selected to be $82 \mu\text{F}$, which is much higher than capacitors C_1 and C_2 placed across the two PV modules. The design details of this converter are available in [32] and Appendix A₂ below.



(a) Practical PV modules and solar simulator system

(b) BCC circuit controlling two serially-connected PV modules



(c) Practical I-V curves of two serially-connected PV modules under various shading cases

Fig. 6. Experimental set-up of BCC integrated with two serially connected PV modules under different shading cases

The experiments were conducted by varying the illumination levels on the two modules to 100% for PV₁ and 40% for PV₂, and the ambient laboratory temperature was varied between 23 °C and 26 °C. The measured I-V curves from these modules are also presented in Fig. 6(c).

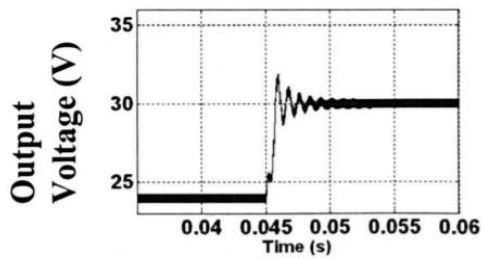
Under the above settings, the device pair S_1 - D_2 of BCC is active to regulate the terminal voltage of PV₁. Four different tests are carried out by applying a step-change in duty ratio K_{11} for the model verification, observing the voltage response across PV₁. As seen from Fig. 6(c), the operating points based on the four test cases are annotated on the two I-V characteristics for modules PV₁ and PV₂, respectively. Case 1 is for points D to C, when K_{11} varying from 0.46 to 0.52 with $\Delta K_{11} = 0.06$, case 2 for B to F, due to duty ratio changing from 0.43 to 0.58, case 3 for E to B, when K_{11} changing from 0.57 to 0.43 and $\Delta K_{11} = -0.14$. For case 4, the corresponding operating point varies from A to G on both I-V characteristics, based on duty ratio changing from 0.40 to 0.59, so $\Delta K_{11} = -0.19$.

Table 1 Experimental parameters of Two PV modules integrated with BCC system.

Parameter	Value
Total output PV power under STC per 1 module	50.05 W
Maximum PV voltage under STC per 1 module	16.5 V
$L_1 = L_2$	2.5 mH
$C_1 = C_2$	26 μ F
C_n	82 μ F
Switching devices	MOSFETs: IRF740 Diodes: DPG10I300PA
Switching Frequency, F_{sw}	20 kHz
Load Resistance, R_L	35 Ω

The four tests show a voltage variation range between 12-18 V. The measured transient responses corresponding to these cases are shown in Fig. 7(b). In comparison, the derived transfer function model parameters in Section 3.1 are set to the same values as those listed in Table 1. Thus, the model is implemented and tested on MATLAB by similarly changing the duty ratio as the experimental test. The transient responses of this model under all four test

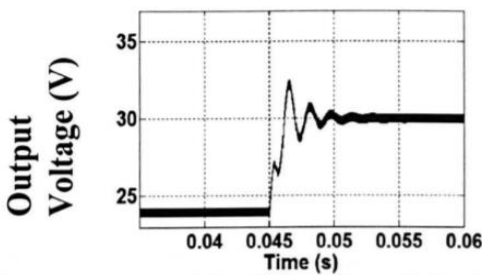
cases are presented in Fig. 7(a). As clearly shown, all practical responses agree well with their corresponding model results.



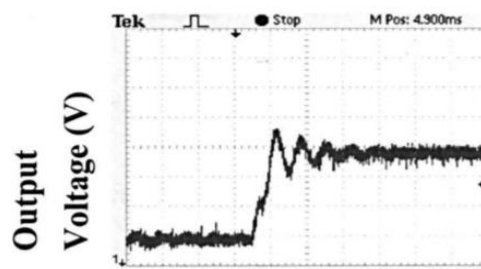
Case 1: Simulated transient response



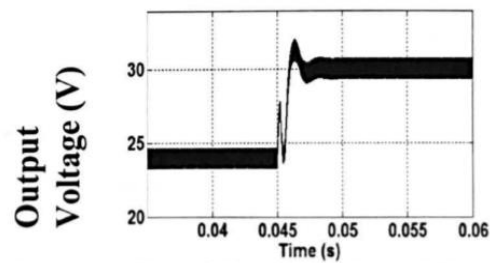
Case 1: Experimental transient response



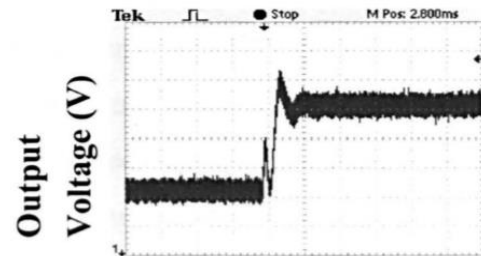
Case 2: Simulated transient response



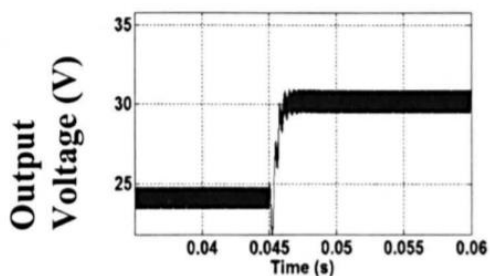
Case 2: Experimental transient response



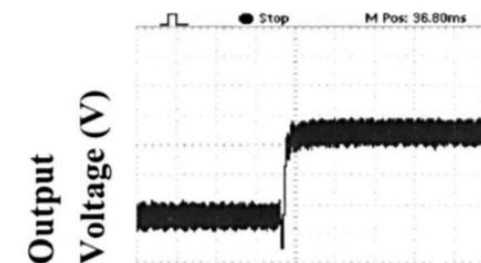
Case 3: Simulated transient response



Case 3: Experimental transient response



Case 4: Simulated transient response



Case 4: Experimental transient response

(a) Simulated PV voltage responses

(b) Experimental PV voltage responses

Fig. 7. Verification of the dynamic mathematical model for a BCC unit under step changes in the sunlight intensity

3.1.2 Experimental Control Verification

Using the experimental prototype shown in Fig. 6, the performance of the MPP control scheme using the BCC modelling-based approach, as described in Section 3, is verified under the conditions of continuously changing sunlight intensity. As shown in Fig.8 five different shading patterns are applied. The experiment is designed to cover the possible operating conditions of the BCC shown in Fig. 4. The BCC converter is controlled by a dsPIC30F4013 microcontroller device, which implements the control scheme and generates the required Pulse Width Modulation (PWM) signal to control the MOSFET switches of the BCC. Measured current and voltage from individual PV modules, PV1 and PV2, including the total power and terminal voltage in response to the light conditions in Fig. 8, are presented in Figs. 9(a) and (b), respectively.

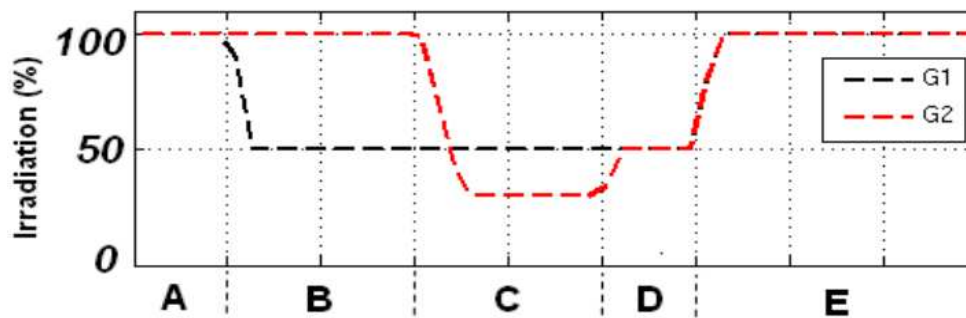
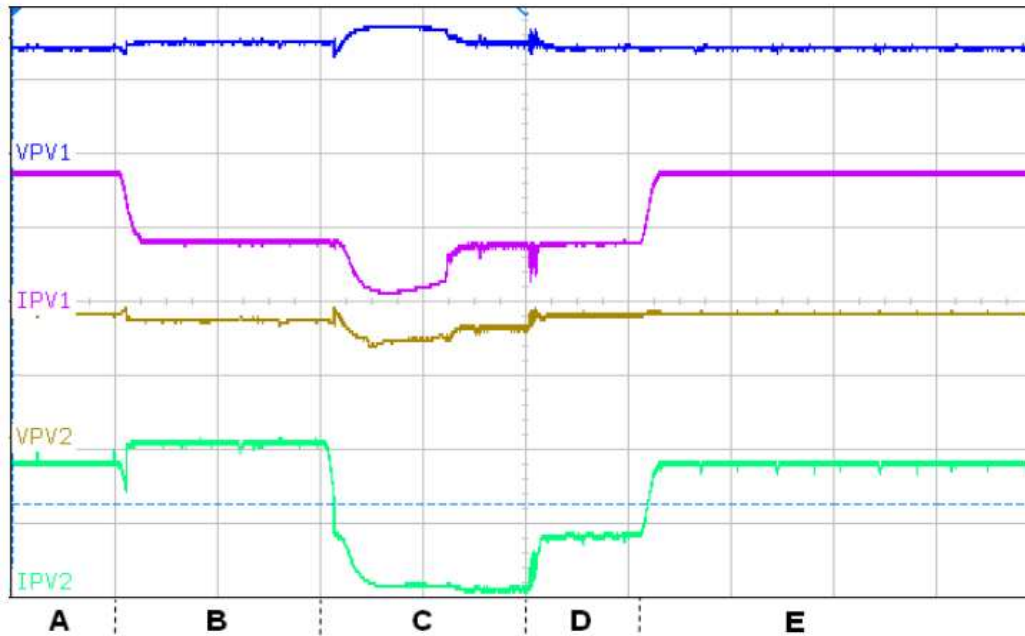


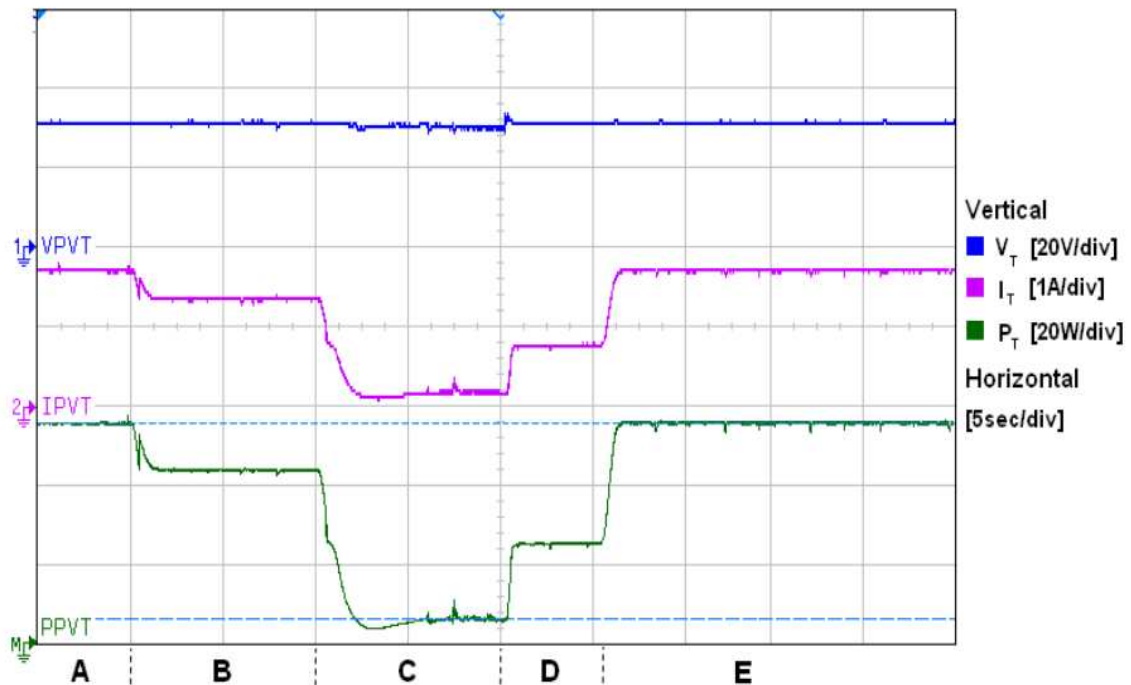
Fig.8. Sunlight intensity changes over time

The experiment starts with scenario A where no shading exists between the two modules, and their corresponding solar irradiances (G_1 & G_2) are equal at 100% producing total power (P_T) of about 55W at 32V terminal voltage ($V_T = V_{PV1} + V_{PV2}$). Thus, the BCC is deactivated, and the power is directly extracted from the modules connected in series. In scenario B, the shading occurs by dimming the light intensity on module PV₁ from 100 to 50%. Under this condition, the difference in solar irradiation between the modules is large enough to activate the switching-pairs S_2 - D_1 ; hence, the MPP tracking controller enables the independent modules to search for their optimum MPP reference voltage values. However, in the scenario C shading, the solar irradiance G_2 over module PV₂ reduces from 100 to 30%, while G_1 is still 50%. Thus, the switching-pairs S_1 - D_2 are now active. The control scheme shows that voltage and current responses, as seen in Fig. 9(a), follow closely their new MPP reference value and settle down to their steady states after about 0.02s. In scenario D, G_2 rises to 50% at the same level as G_1 ; thus, the total current increases compared to the previous scenario leading to a rise in the terminal power, as shown in Fig. 9(b). Finally, both light intensities increase from 50 to

100% simultaneously, indicating complete cessation of shading. Therefore, the currents generated by the two modules increase, causing a significant increase in the total power to the maximum power point, similar to that produced in scenario A.



(a) Measurements of modules PV1 and PV2 under dynamic change in solar irradiation



(b) Terminal Power, Current and Voltage measurements of a BCC controlling two PV modules under dynamic change in solar irradiation

Fig.9. Voltage, Current and Power measurements of a practical system consisting of a BCC controlling two serially-connected PV modules

4. Simulation Results & Discussions

The proposed combined array scheme is tested via the MATLAB-SIMULINK platform under non-uniform shading conditions. The latter is modelled by five shading conditions, namely Long-Narrow (LN), Long-Wide (LW), Short-Narrow (SN), Short-Wide (SW), and dynamic shadings. The performance of the proposed scheme is compared to the existing reconfiguration methods, such as MS-EC and IE alone and the conventional TCT configuration using only bypass diodes. The comparison is made based on various performance parameters, i.e., total power extracted, Mismatch Power Loss (%*ML*), Efficiency (% η), system complexity and the payback return. The combined system specifications are listed in Table 2. The maximum power generated by the total array system is 1873.8 W under unshaded conditions, where the irradiance is 1000 W/m² for all modules and the temperature is 25 °C.

Table 2 Specifications of 1.87 kW combined scheme integrated 6x6 PV array system.

Parameters		Symbols	Values
For a single PV module	No. series cells	N_s	40
	No. parallel cells	N_p	1
	Maximum power at $T = 25^\circ\text{C}$ and $G = 1000 \text{ W/m}^2$	P_{MPP}	52.05 W
	MPP voltage at $T = 25^\circ\text{C}$ and $G = 1000 \text{ W/m}^2$	V_{MPP}	18.18 V
Rated bus voltage		V_{Bus}	112 V
Switching frequency		F_{sw}	20 kHz
Inductors	IBC and DPPs	$L_F, L_1, L_2,$	8 mH
	BCCs	L_{11}, L_{21}, L_{12} and L_{22}	8 mH
Capacitors	IBC and DPPs	C_{TF}	35 μF
		$C_F, C_{T1},$ and C_{T2}	20 μf
	BCCs	C_{n1} and C_{n2}	10 μF
		C_1, C_2, C_3 and C_4	20 μF
P+I controllers for inner converters BCC₁ & BCC₂	Proportional gains	K_{p1} and K_{p2}	0.001
	Integral gains	K_{i1} and K_{i2}	4.69
P+I controllers for Front-End converter	Proportional gain	K_{p3} and K_{p4}	0.5×10^{-3}
	Integral gain	K_{i3} and K_{i4}	2
P+I controllers for outer DPP converters DPP₁ & DPP₂	Proportional gains	K_{p5} and K_{p6}	0.5×10^{-6}
	Integral gains	K_{i5} and K_{i6}	4

4.1. Long-Narrow shading (LN)

In this shading pattern, the first two columns are shaded, where the serially connected modules within each column (i.e. string) receive varying sunlight intensity levels, as seen in Fig. 10(a). Also, Figs. 10(b)-(d) illustrate the combined scheme procedure.

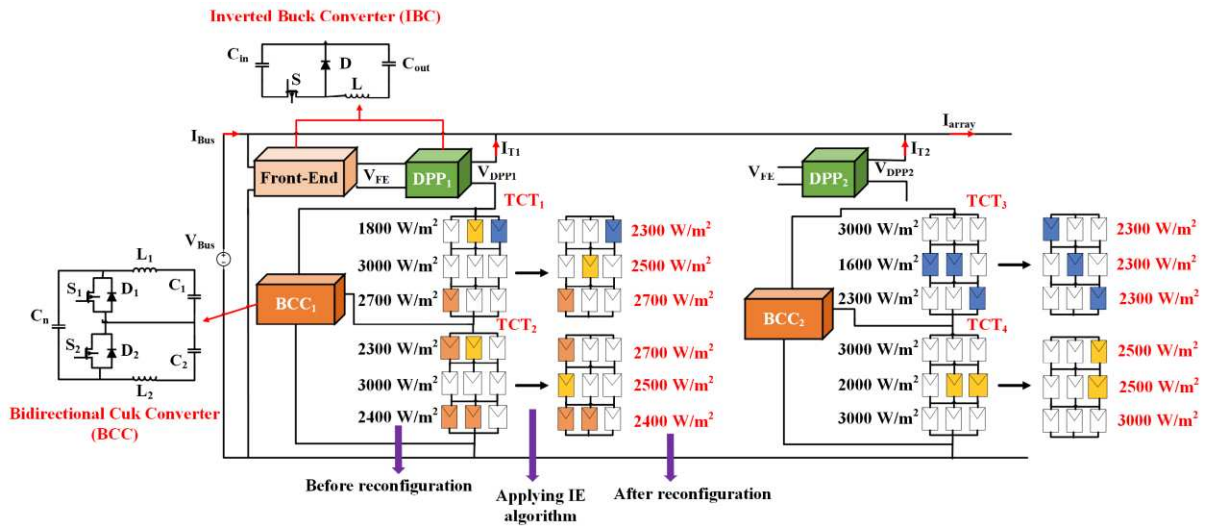
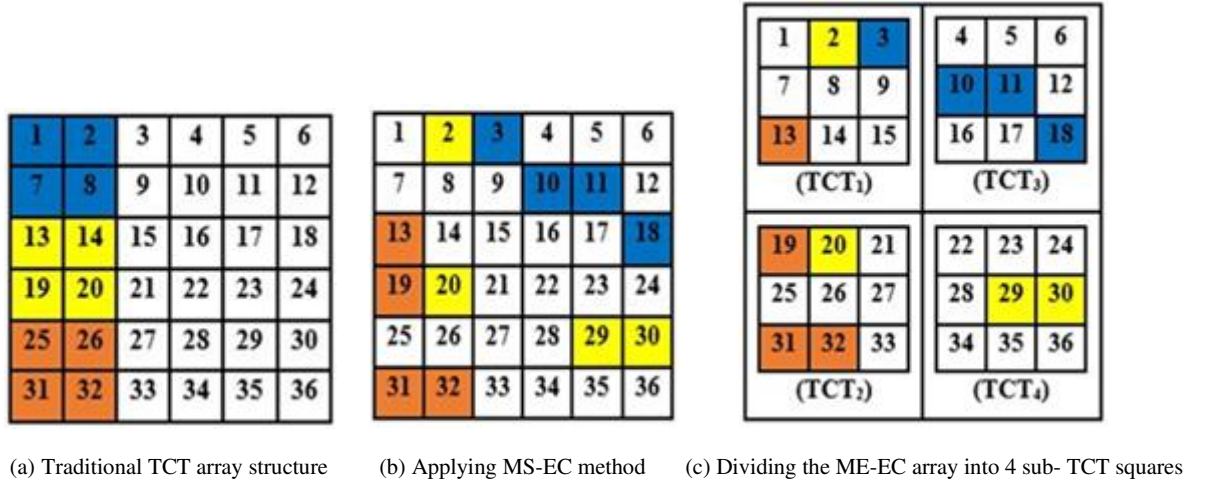
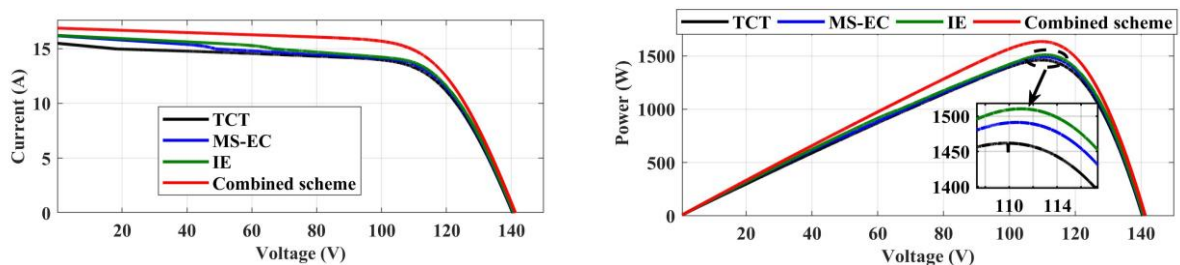


Fig. 10. The implementation procedure of the combined scheme technique for a 6x6 array system under LN shading

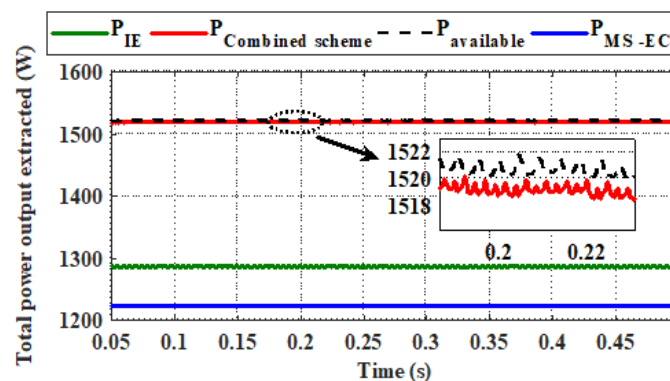
The current and power extracted from each scheme under the LN shade pattern are presented in the I-V and P-V characteristics, including the total power generated versus time in Fig. 11. Results reveal that the proposed combined scheme produces the highest output power of 1635 W, as shown in Figs. 11(b) and (c), respectively, followed by the two reconfiguration techniques, MS-EC and IE, at 1491 W and 1511 W. However, the conventional TCT array with only bypass diodes gives the lowest power of 1223 W. The benefit of applying the combined scheme is evident due to that it increases the current generated from individual

sub-TCT squares, as seen in Fig. 11(a). This is as a result of employing BCC-DPP converters for accurate MPP tracking. Only a single power peak is present on the P-V curve of the combined scheme, as shown in Fig. 11(b). Following the control scheme presented in Section 3, the switching-pair devices S_1-D_2 and S_3-D_4 are both activated for the two inner BCCs. This firstly causes the sub-TCT voltages to be adjusted appropriately by regulating the duty ratios of the inner BCCs. After about 0.08 s, the terminal voltages of the four sub-TCT groups (i.e., V_{TCT1} , V_{TCT2} , V_{TCT3} and V_{TCT4}) closely follow their respective new MPP reference values of 53.72 V, 53.81V, 54.37 V and 53.2 V, as seen in Figs. 12(a)-(h). The proposed topology has recorded the lowest Mismatch Loss, ML of 0.43 %, and hence, it increased the total power by 11.83%, 9.66% and 8.21% compared to the TCT, MS-EC and IE, respectively.



(a) I-V curves of a 6×6 PV array system

(b) P-V curves of a 6×6 PV array system



(c) Comparison of the simulated maximum power extracted responses between the combined scheme and existing methods

Fig. 11. P-V, I-V characteristics, and simulated power responses of the combined scheme and other existing reconfiguration techniques under LN shading

4.2. Long-Wide shading (LW)

Under this pattern, more PV modules are affected by different illumination levels than those in the previous shading case, as seen in Fig. 13(a). The complete reconfiguration process of the system is illustrated in Figs. 13(b)-(d). The simulated P-V, I-V characteristics and power

responses of the combined scheme are compared to those obtained using the traditional TCT and the other two reconfiguration techniques, as seen in Fig. 14.

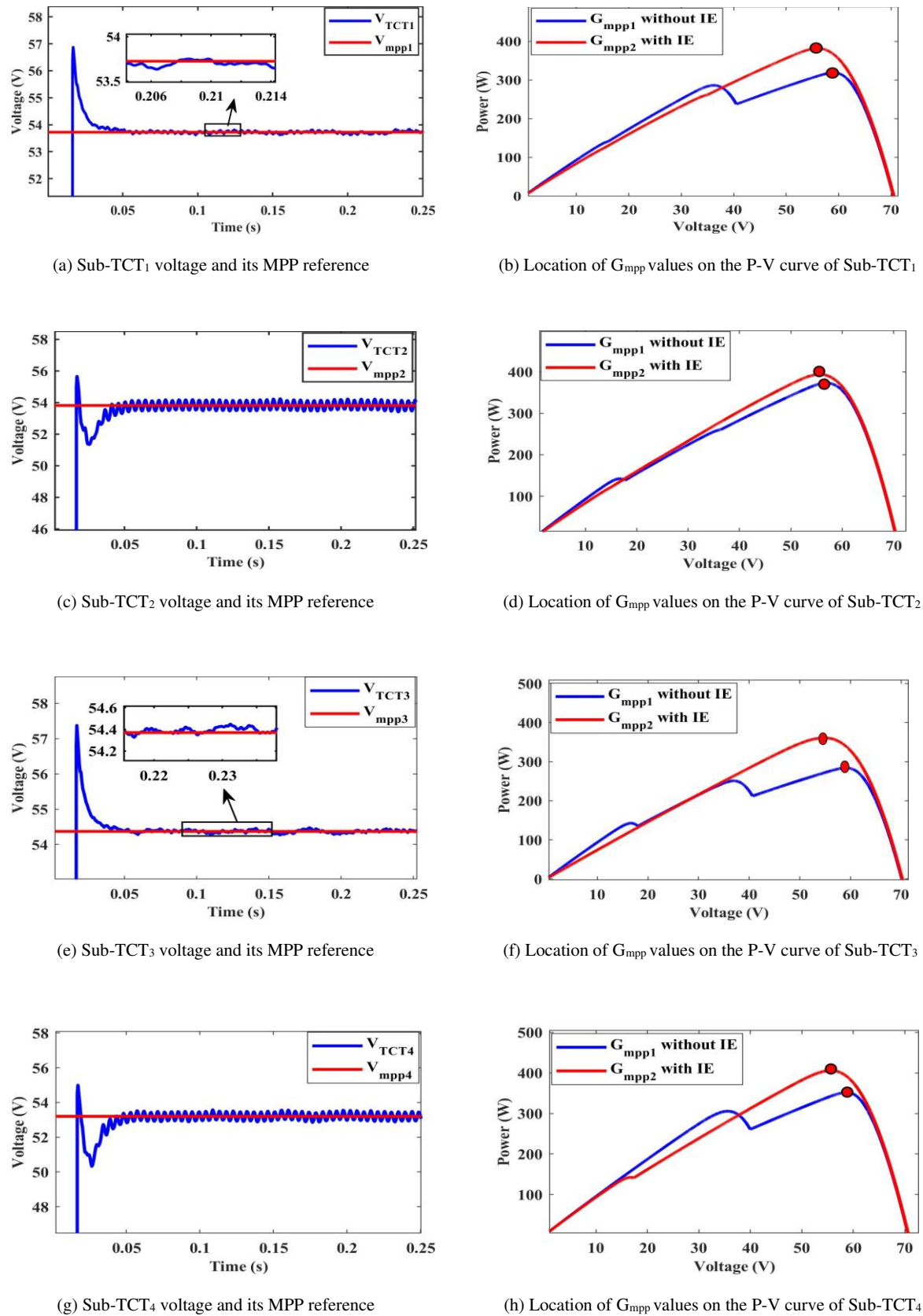


Fig. 12. Simulated voltage responses of the sub-TCT array groups and their corresponding P-V curves under LN shading

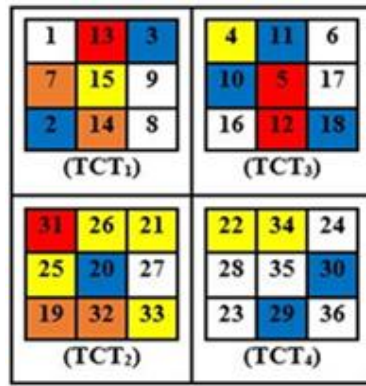
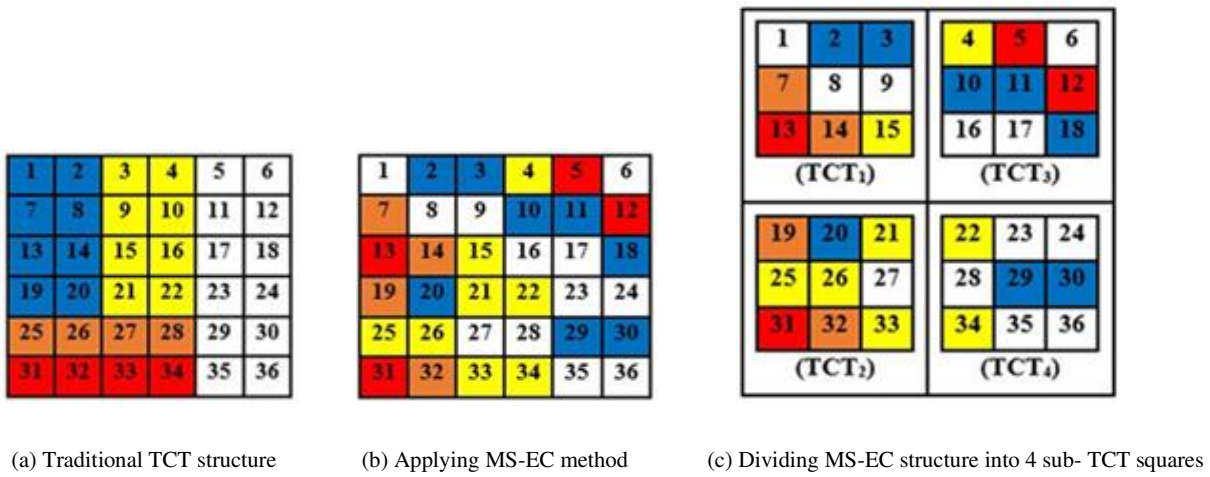
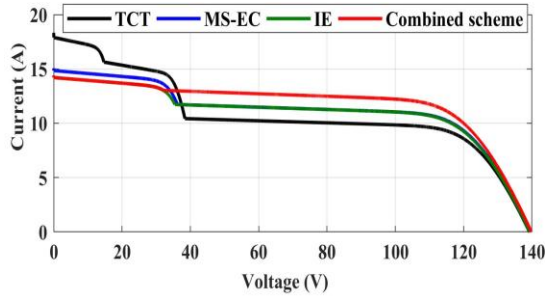
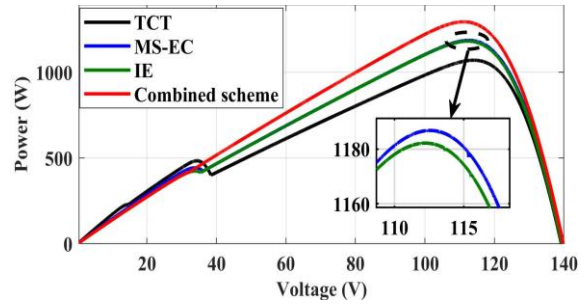


Fig. 13. The implementation procedure of the combined scheme technique for a 6x6 array system under LW shading

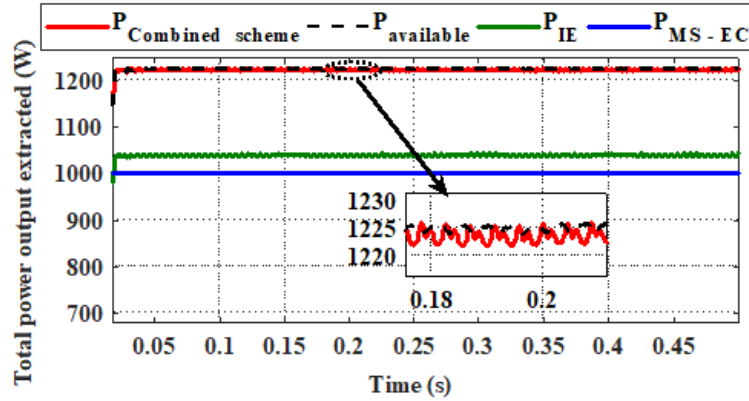
The combined scheme for this system is shown to have the best power performance, with a total power of 1295 W and an ML of 1.22%. This is followed by the MS-EC scheme alone generating 1187 W, as seen in Figs. 14(b)-(c), and having ML of 9.46%. On the other hand, the conventional TCT array again showed the lowest power performance; its P_{TCT} is 20.92% and 10.92% less than that of the combined system and MS-EC. The corresponding MPP values for all sub-TCT square groups are (324.1 W, 6.116 A), (279.7 W, 5.436 A), (326.7 W, 6.136 A) and (294.4 W, 5.536 A), respectively. The control scheme can still cause a transition of all the TCT sub-array voltages to their new MPP values after a small disturbance. The benefit of the combined method can be clearly observed such that the individual P-V curves of the four sub-TCT groups, as seen in Figs. 15(a)-(h), exhibit almost a single power peak, leading to an accurate and straightforward MPP tracking.



(a) I-V curves of a 6x6 PV array system



(b) P-V curves of a 6x6 PV array system



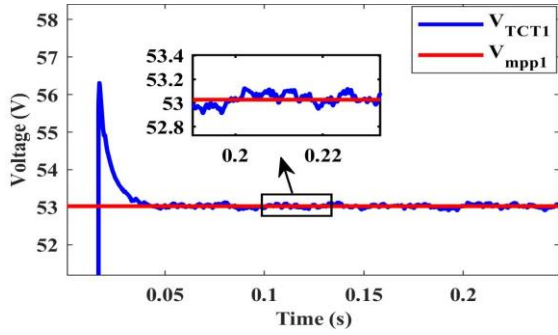
(c) Comparison of the simulated maximum power extracted responses between the combined scheme and existing methods

Fig. 14. P-V, I-V characteristics, and simulated power responses of the combined scheme and other existing reconfiguration techniques under LW shading

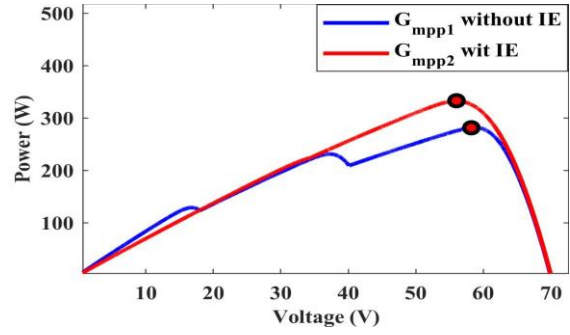
4.3. Short-Narrow shading (SN)

Results are shown in the same format for the SN shading case in Figs. 16, 17 and 18, respectively.

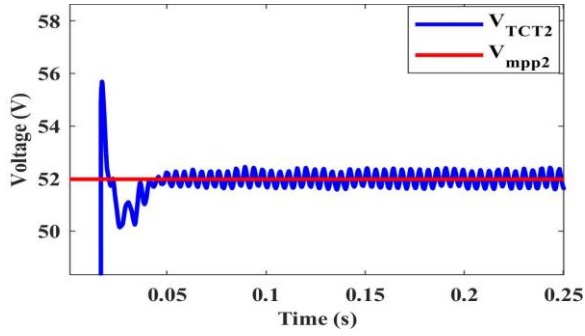
The combined scheme again has the highest P_{array} of 1723 W, as shown in the P-V curve in Fig. 17(b). P_{array} of MS-EC and IE reconfiguration techniques is lower than that of the combined scheme by more than 11.38% and 6.56%. The simple TCT has the lowest P_{TCT} value of 1397 W. With the MPP tracking converters scheme, the individual voltages of the sub-TCT arrays are again controlled to their respective MPP values despite small disturbances, as shown in Fig. 18, but V_{TCT3} is regulated to the value estimated by the MPP model as expected. Hence, this sub-group unit remains unchanged after applying the IE algorithm. The proposed scheme is still considered the most efficient configuration under this SN pattern by presenting the lowest ML of 0.63%. In comparison, Both MS-EC and IE, along with TCT schemes, have ML s of 10.78%, 6.74% and 19.43%, respectively.



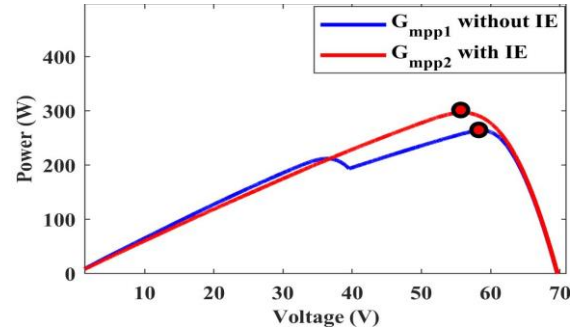
(a) Sub-TCT₁ voltage and its MPP reference



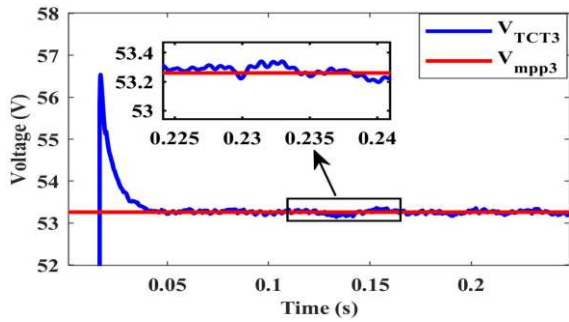
(b) Location of G_{mpp} values on the P-V curve of Sub-TCT₁



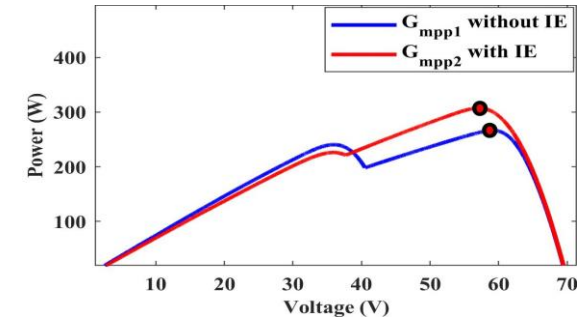
(c) Sub-TCT₂ voltage and its MPP reference



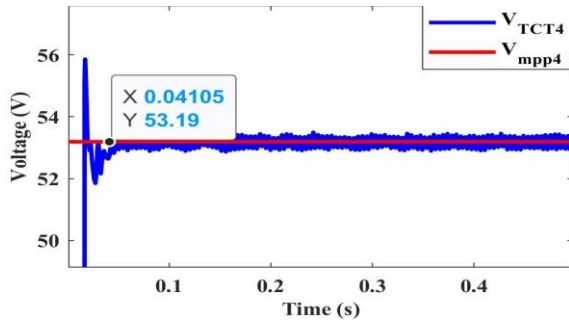
(d) Location of G_{mpp} values on the P-V curve of Sub-TCT₂



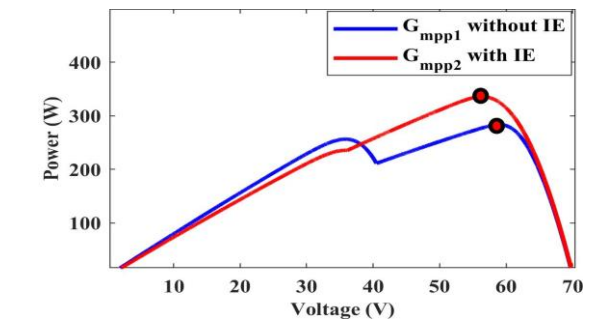
(e) Sub-TCT₃ voltage and its MPP reference



(f) Location of G_{mpp} values on the P-V curve of Sub-TCT₃



(g) Sub-TCT₄ voltage and its MPP reference



(h) Location of G_{mpp} values on the P-V curve of Sub-TCT₄

Fig. 15. Simulated voltage responses of the sub-TCT array groups and their corresponding P-V curves under LW shading

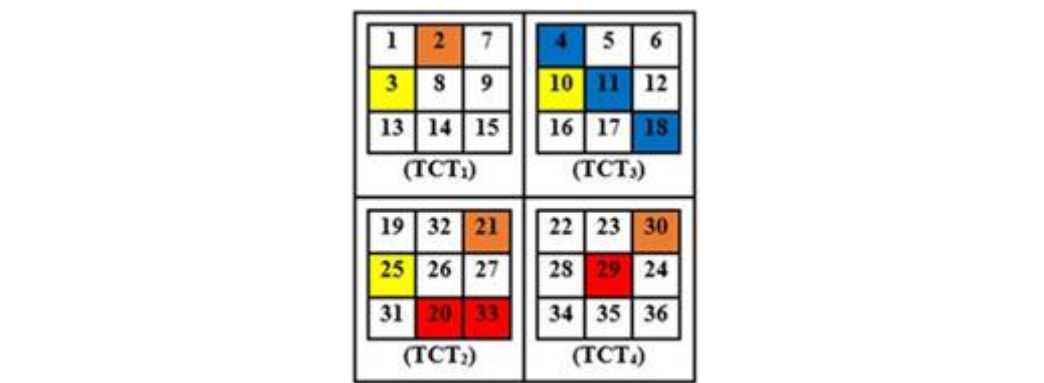
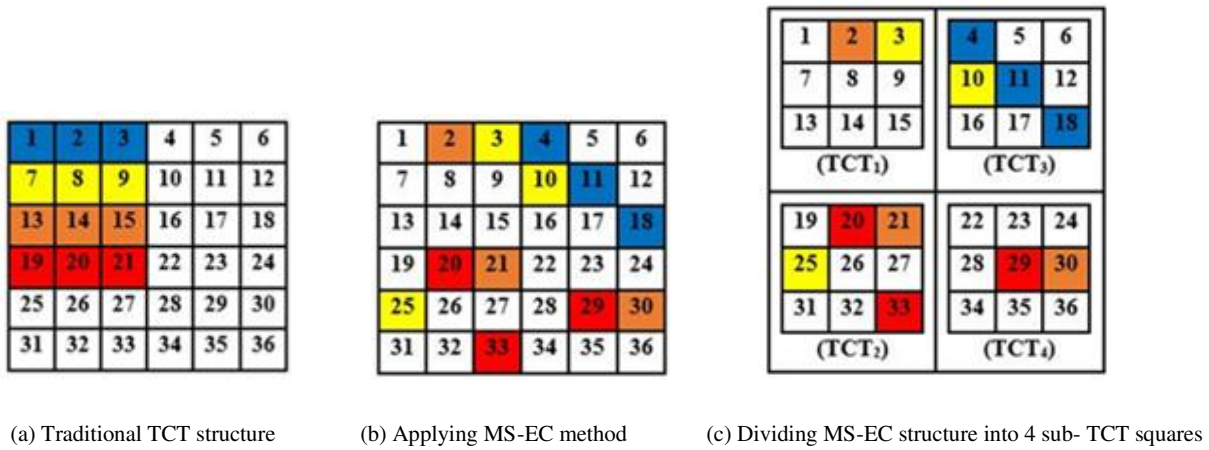


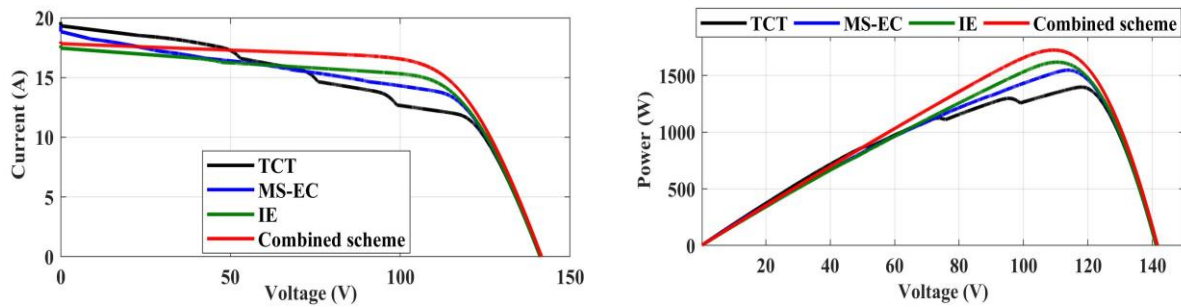
Fig. 16. P-V, I-V characteristics, and simulated power responses of the combined scheme and other existing reconfiguration techniques under LW shading

4.4. Short-Wide shading (SW)

The light intensity for this shading pattern is shown in Fig. 19(a). Other results follow the same procedures as before and are shown in Figs. 19(b)-(d), and Figs. 20 and 21.

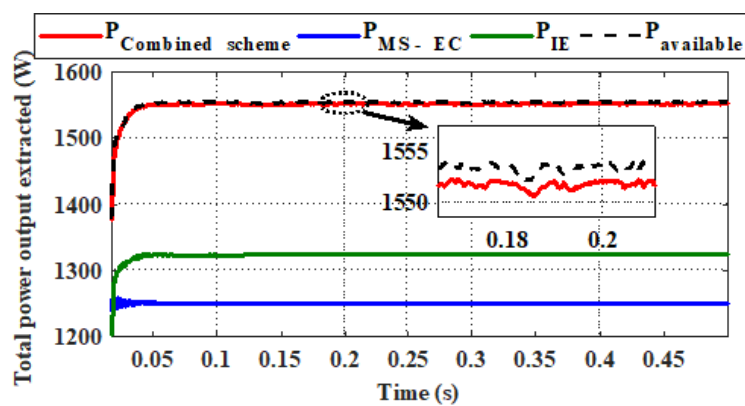
As seen from Figs. 20(b) and (c), combined and TCT schemes have shown lower power output values than those of the previous shading patterns. The proposed scheme has the highest P_{array} of 1277 W while it is 857.7 W, 1228 W and 1243 W in TCT, MS-EC and IE configurations. The combined scheme is the most efficient configuration under this shading pattern as it presents the lowest ML of 0.26%, while TCT has the highest ML of 33.01%. After the four sub-TCT array groups have been reconfigured using the IE method, the control system can still quickly enable the four TCT units to restore to their optimal PV array operation, as seen in Figs. 21(a)-(h). This pattern has recorded the highest power improvement among the other patterns; hence, the combined scheme system increased the total array power output by

48.89% compared to that obtained using the traditional TCT array structure with only bypass diodes.



(a) I-V curves of a 6x6 PV array system

(b) P-V curves of a 6x6 PV array system



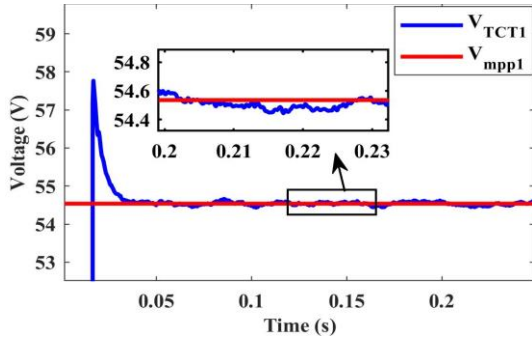
(c) Comparison of the simulated maximum power extracted responses between the combined scheme and existing methods

Fig. 17. P-V, I-V characteristics, and simulated power responses of the combined scheme and other existing reconfiguration techniques under SN shading

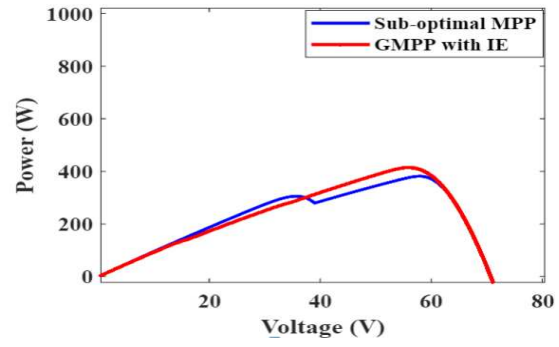
4.5. A Dynamic Change in Solar Irradiation with Time

In this study, the shading patterns on the PV modules tested change with time. In particular four modules, PV_{21} , PV_{27} , PV_{29} and PV_{34} , respectively, are randomly shaded and their respective sunlight intensity levels (G_{21} , G_{27} , G_{29} and G_{34} , respectively) all have a step-change at different time intervals throughout the day, as seen in Fig. 22. The shading change is categorised into four patterns as follows:

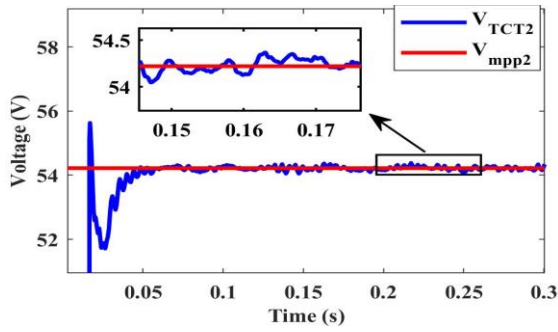
- **Pattern 1:** Modules PV_{21} , PV_{27} , PV_{29} and PV_{34} are initially illuminated at 300 W/m^2 , 500 W/m^2 and 700 W/m^2 , respectively.
- **Pattern 2:** A step-change in solar irradiance occurs at 0.1 s; G_{21} of module PV_{21} changing from 300 W/m^2 to 100 W/m^2 while G_{34} of PV_{34} from 700 W/m^2 to 500 W/m^2 .



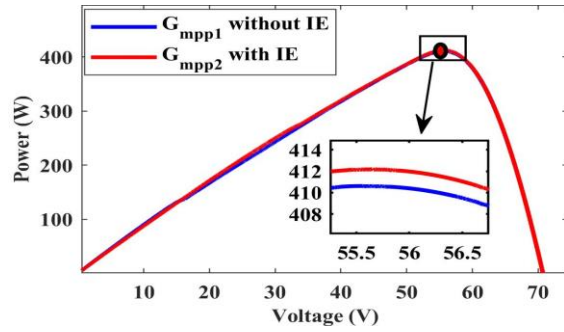
(a) Sub-TCT₁ voltage and its MPP reference



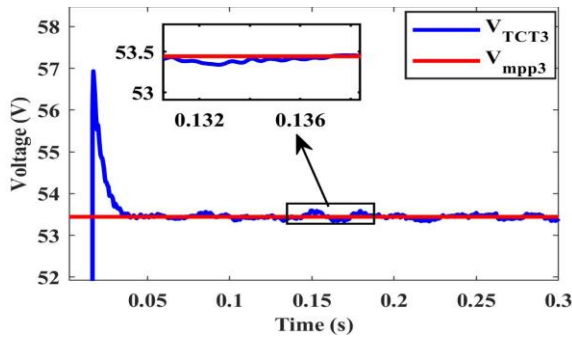
(b) Location of G_{mpp} values on the P-V curve of Sub-TCT₁



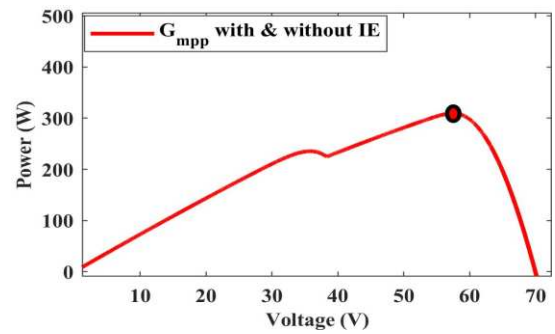
(c) Sub-TCT₂ voltage and its MPP reference



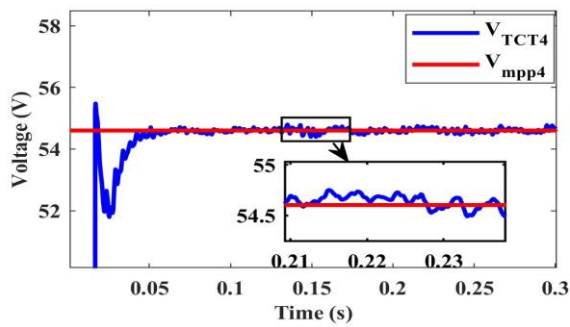
(d) Location of G_{mpp} values on the P-V curve of Sub-TCT₂



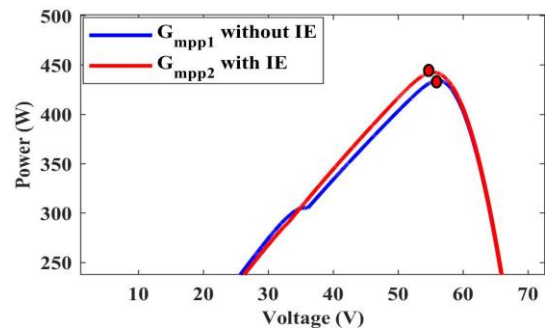
(e) Sub-TCT₃ voltage and its MPP reference



(f) Location of G_{mpp} values on the P-V curve of Sub-TCT₃



(g) Sub-TCT₄ voltage and its MPP reference



(h) Location of G_{mpp} values on the P-V curve of Sub-TCT₄

Fig. 18. Simulated voltage responses of the sub-TCT array groups and their corresponding P-V curves under SN shading

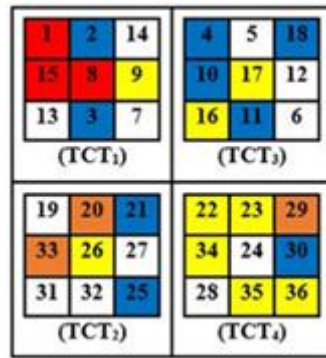
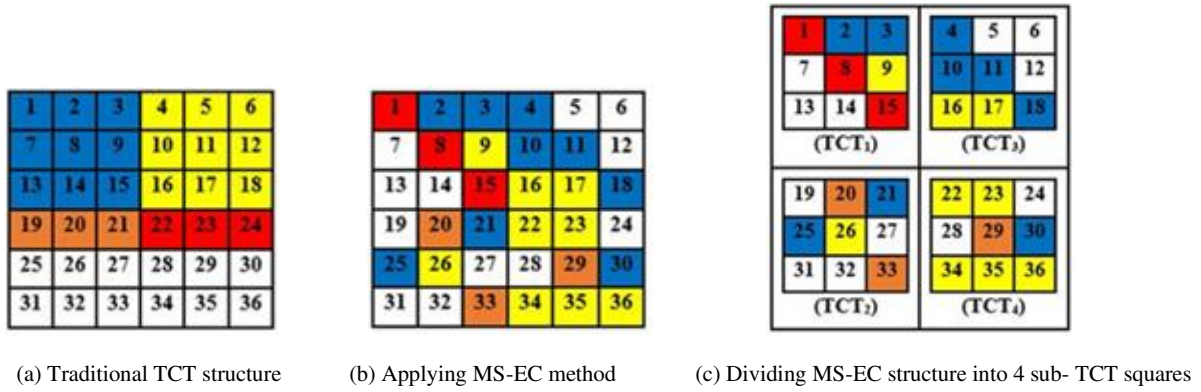


Fig. 19. The implementation procedure of the combined scheme technique for a 6x6 array system under SW shading

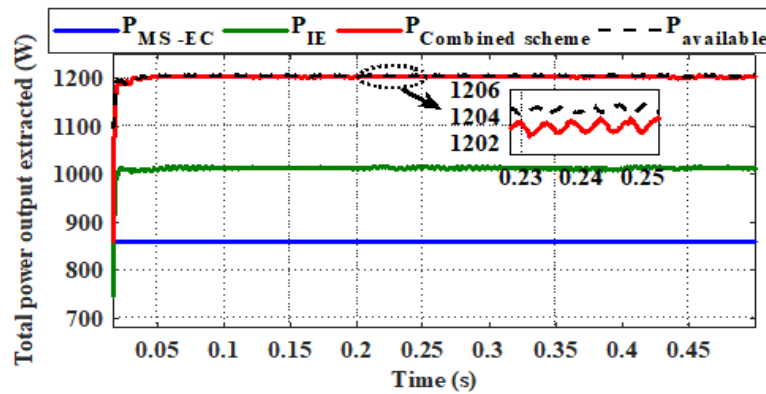
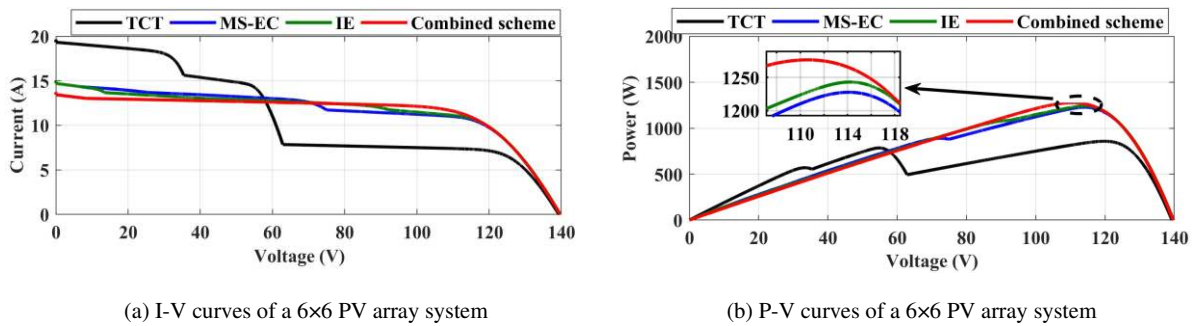
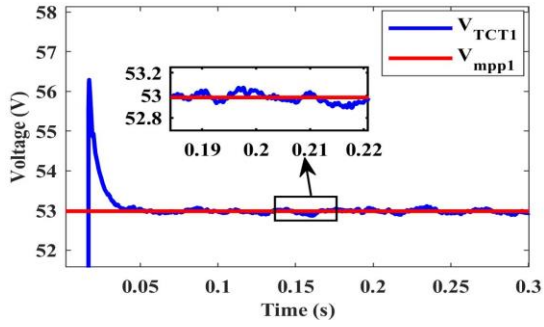
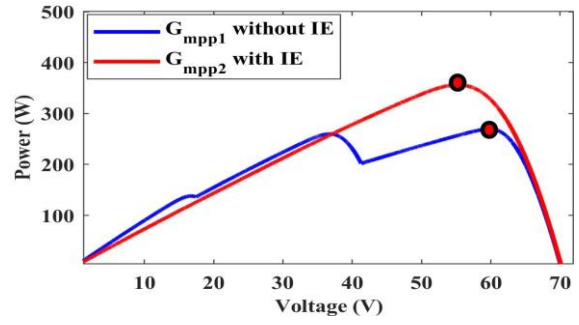


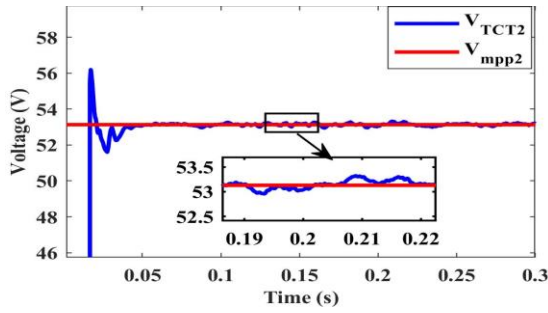
Fig. 20. P-V, I-V characteristics, and simulated power responses of the combined scheme and other existing reconfiguration techniques under SW shading



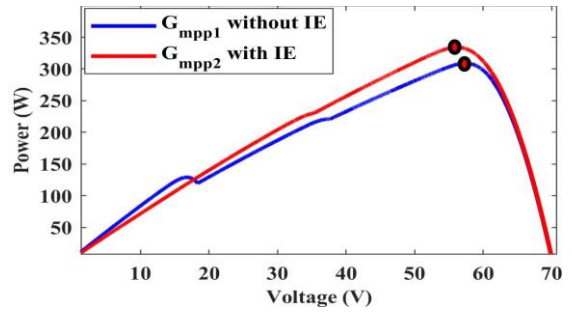
(a) Sub-TCT₁ voltage and its MPP reference



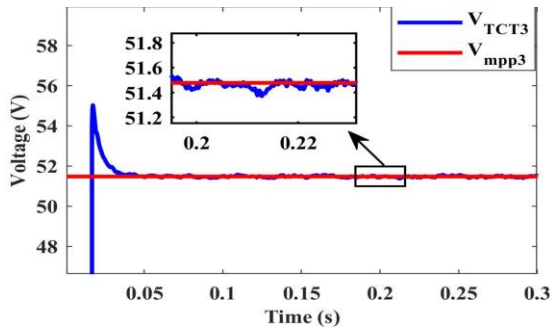
(b) Location of G_{mpp} values on the P-V curve of Sub-TCT₁



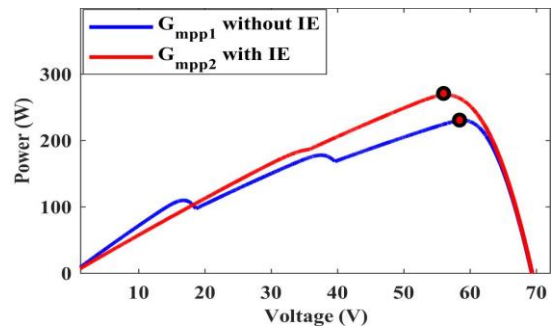
(c) Sub-TCT₂ voltage and its MPP reference



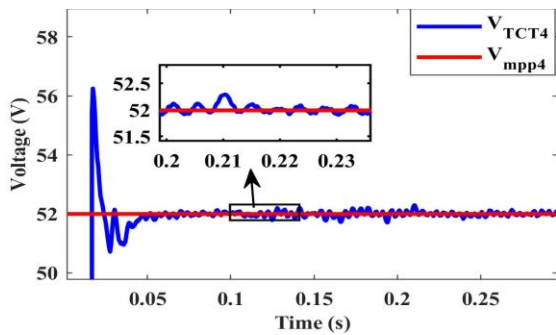
(d) Location of G_{mpp} values on the P-V curve of Sub-TCT₂



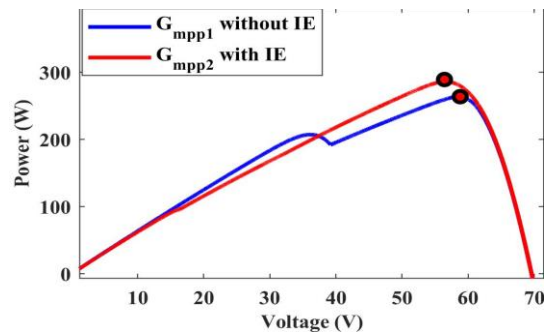
(e) Sub-TCT₃ voltage and its MPP reference



(f) Location of G_{mpp} values on the P-V curve of Sub-TCT₃



(g) Sub-TCT₄ voltage and its MPP reference



(h) Location of G_{mpp} values on the P-V curve of Sub-TCT₄

Fig. 21. Simulated voltage responses of the sub-TCT array groups and their corresponding P-V curves under SW shading

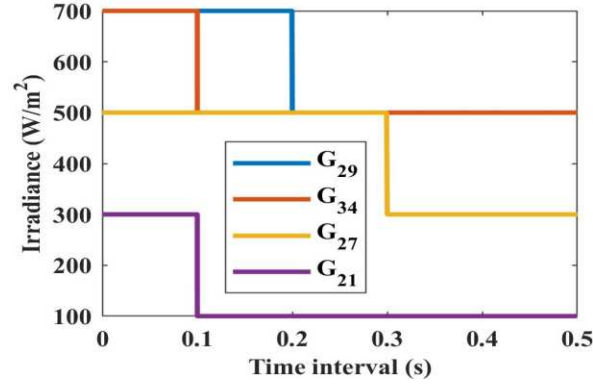


Fig. 22. Dynamic change of sunlight intensity levels for modules PV₂₁, PV₂₇, PV₂₉ and PV₃₄, respectively at various time intervals

- **Pattern 3:** A step-change in the solar irradiance occurs at 0.2 s, G_{29} of module PV₂₉ from 700 W/m² to 500 W/m².
- **Pattern 4:** A step-change in the solar irradiance, G_{27} of module PV₂₇ from 500 W/m² to 300 W/m² occurs at 0.3 s.

The voltage responses of the individual sub-TCT square arrays are presented in Figs. 23(a-d) and the corresponding total output power responses of each technique are depicted in Fig. 24. Detailed explanations are summarised as follows:

- 1) **From $t = 0$ to $t = 0.1$ s,** PV₂₁ always receives the lowest solar irradiation while the light intensities on PV₃₄ and PV₂₉ are equal and that on PV₂₇ is the highest. The MPP model, described in section 3, is applied to predict the maximum PV powers of each sub-TCT group along with their corresponding total voltages. Hence, the switch pairs S_1 - D_2 of BCC₁ are active while S_4 - D_3 of BCC₂ should be activated. This prompts both control schemes for inner and outer DPPs to regulate the duty ratios until the MPP voltages are achieved. Following this pattern, all TCT array voltages (Figs. 23(a)-(d)) take about 0.04 s to recover to their original states.
- 2) **From $t = 0.1$ to $t = 0.2$ s,** PV₃₄ experiences a drop in the solar insolation to 500 W/m² at 0.1 s while that on PV₂₁ decreases to 100 W/m². Thus, the illumination levels of PV₂₇ and PV₂₉ remain unchanged. In this case, the switching states of both BCC₁ and BCC₂ are kept the same as they were in the previous case, and the control system can quickly adjust the duty ratios for all PV sub-array squares to reach the optimal operation. Therefore, V_{TCT2} (Fig. 23(b)) and V_{TCT3} (Fig. 23(c)) are both regulated to the new values estimated by the MPP model as expected while V_{TCT1} (Fig. 23(a)) and V_{TCT4} (Fig. 23(d)) are maintained to their original values for MPP generation after a small perturbation.

- 3) From $t = 0.2$ to $t = 0.3$ s, PV_{29} experiences a step decrease in its solar irradiance at $t = 0.2$ s, active switch pairs in BCC_2 becomes S_3-D_4 , while that in BCC_1 is unchanged. As shown in Fig. 23(d), V_{TCT4} is controlled to its desired level in about 0.05 s while V_{TCT1} , including V_{TCT2} and V_{TCT3} (Figs. 23(a)-(c)) maintain their original values even though they are disturbed due to the operating point variations.
- 4) From $t = 0.3$ to $t = 0.5$ s, G_{27} starts to drop significantly at $t = 0.3$ s. Subsequently, the control actions are taken, and a response with a small voltage fluctuation is obtained for V_{TCT1} , see (Fig. 23(a)). Thus, the proposed control scheme is considered as robust as expected upon every detection to the variations of shading conditions.

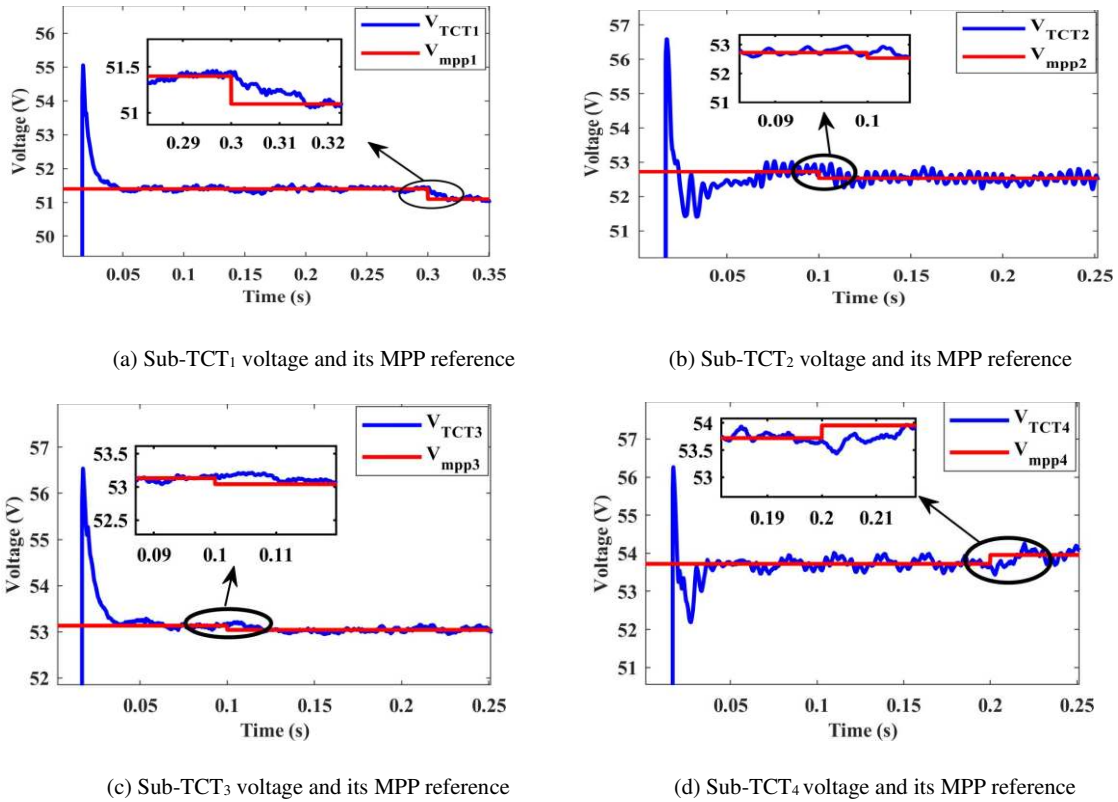


Fig. 23. Simulated voltage responses of the sub-TCT array groups under a dynamic change in solar irradiation

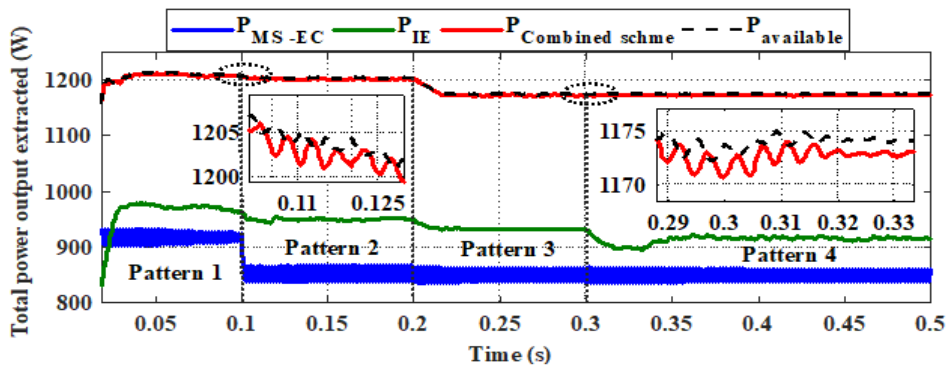


Fig. 24. Simulated power responses of the combined scheme and other existing reconfiguration techniques under a dynamic change in solar irradiation

4.6. Summary of the obtained results

From the data depicted in Figs. 25-27, the power gain variations of the combined scheme over the conventional TCT array with bypass diodes range from 11 to 21% under column-wise shading, which is the case in the LN and LW patterns. As the shading level sharply increases (i.e., as shown in SN and SW patterns), the power gain and efficiency increase while the mismatch loss ($ML\%$) is almost negligible. The maximum calculated efficiency for the combined scheme is 99.74% when PV modules within the array are under the SW pattern. This shows that the combined scheme structure can deliver power as much as 48.89% higher than the traditional TCT array configuration with only bypass diodes.

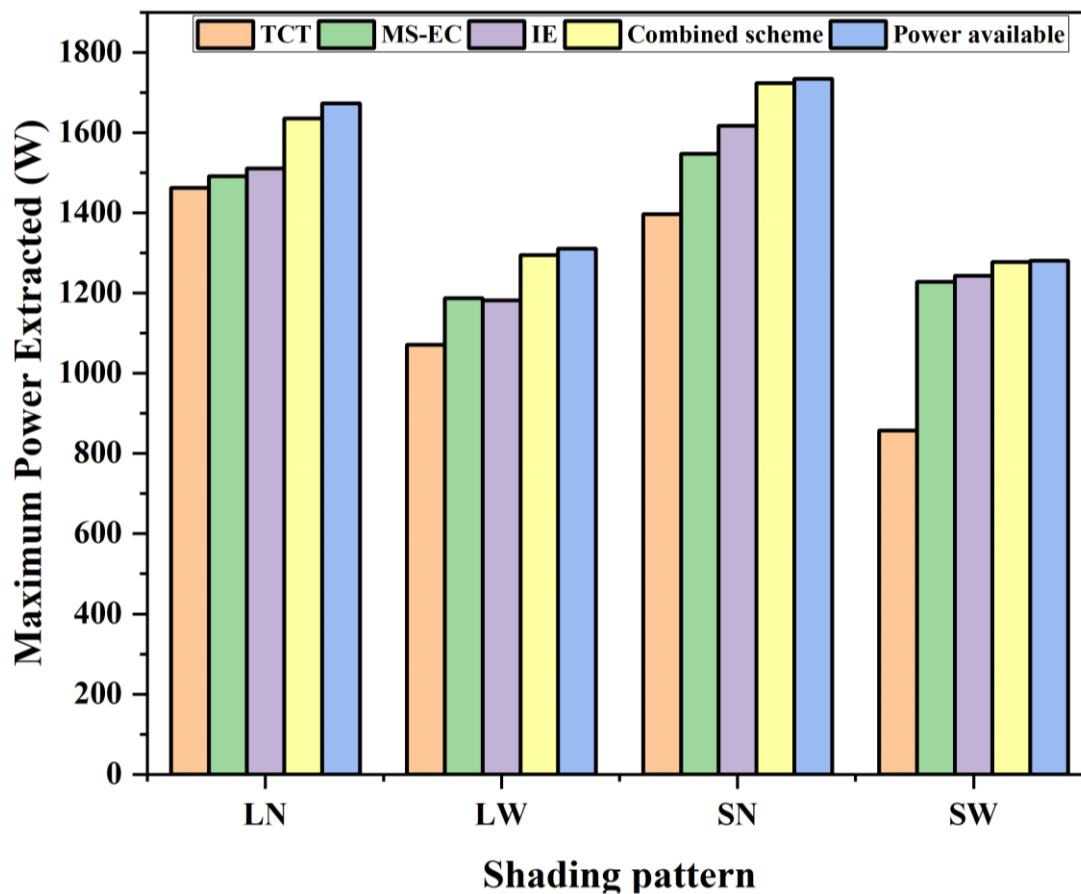


Fig. 25. Comparison of the total maximum power generated using different reconfiguration schemes under PSCs

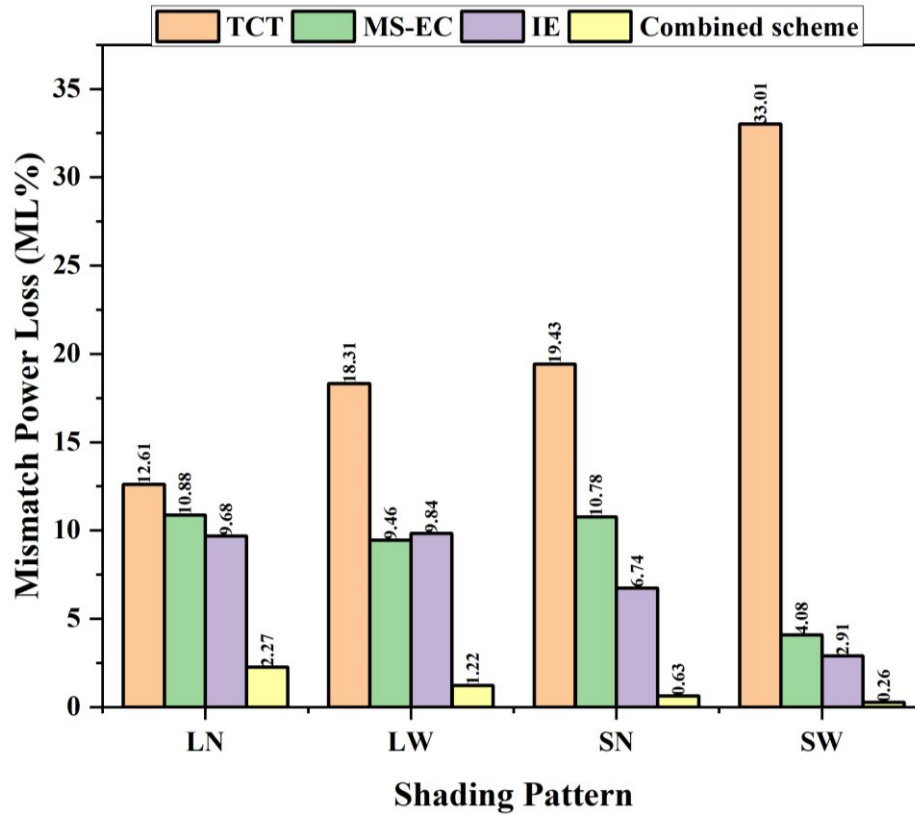


Fig. 26. Comparison of the mismatch power loss ($ML\%$) of different reconfiguration schemes under PSCs

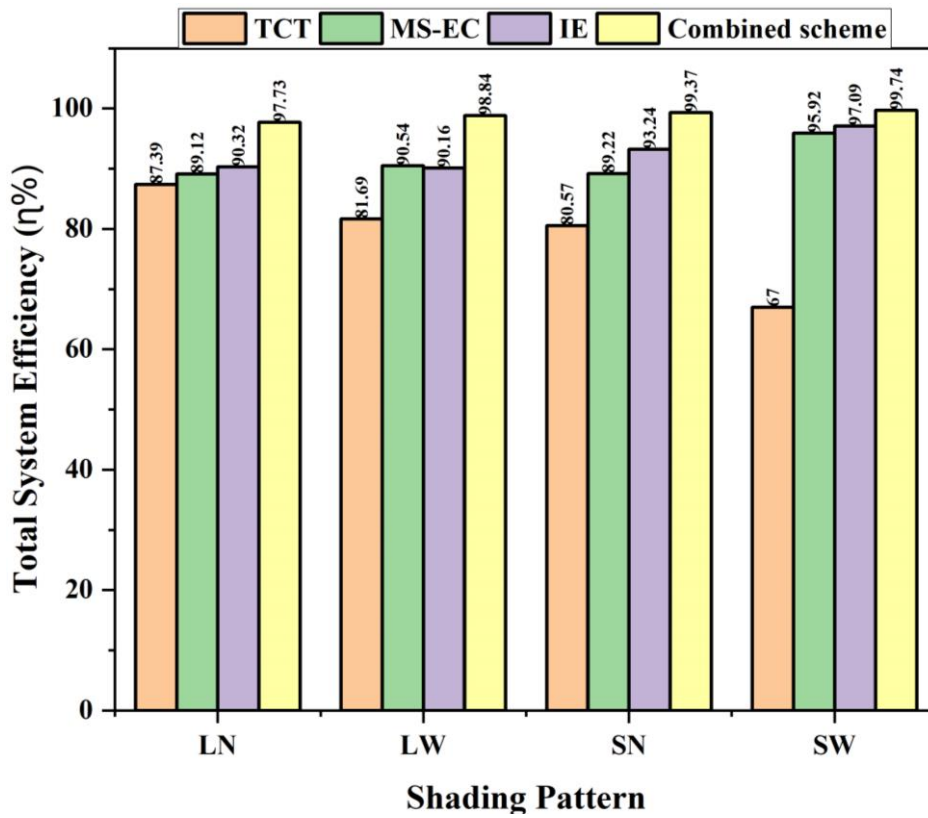


Fig. 27. Comparison of the total system efficiency ($\eta\%$) of different array reconfiguration schemes under PSCs

Table 3 presents a thorough, complete comparative analysis between the existing techniques in literature and the proposed combined scheme for a PV array system under partial shading conditions. Various parameters are considered for this comparative study, such as efficiency, the requirements of switching active devices, performance under different shading patterns, system complexity and complexity of the reconfiguration algorithms. Although MS-EC and IE are much simpler to implement, they both exhibit limitations in requiring a skilled person to perform the physical changes for the modules within the PV array. They also cause extra power losses due to either the long cabling requirements for MS-EC or the IE's additional switching devices and sensors. Therefore, none of the former schemes can ensure maximum power generation under PSCs. Moreover, the combined system can be complex and costly due to the converters and the switches involved in this technique. On the other hand, the benefit in payback returns using the proposed combined method can be noticed by showing power improvements between 23 and 48% and an average efficiency of 98.91% for an accurate MPP tracking under PSCs.

Table 3 Quantitative analysis of different performance parameters and their comparison between the proposed combined scheme, MS-EC, IE and TCT existing schemes under PSCs.

Performance parameter	Combined-Scheme	MS-EC	IE	TCT
Efficiency ($\% \eta$)	Very High	High	High	Medium-Low
Requirements of active switching devices for 6x6 PV array size	64 switches	0	72 switches	0
Improvements of power extraction	Very High	Medium-High	Medium-High	Low
Complexity	Complex	Low	Medium	Low
Shade dispersion	Very High	Medium	Medium-High	None
Use for large arrays	Highly efficient	Efficient	Efficient	Least Efficient
Mismatch power loss ($\% ML$)	Very low	Low-Medium	Low-Medium	Very High
Altering electrical connections is required	Yes	No	Yes	No
Sensors	Yes	No	Yes	No

5. Conclusion

This paper presented a novel combined approach for reconfiguration of a TCT-interconnected PV array and optimising its output power under non-uniform irradiation conditions. The three combined techniques were a modified MS-EC and IE algorithms and BCC-DPP power processing. The proposed scheme has shown to offer the following

advantages over the existing techniques: 1) effective distribution of the shading effect all over the array by relocating the PV modules at greater distances from their former neighbours, using the MS-EC algorithm; 2) increased power generation by using the IE algorithm via equalising the irradiation levels over the rows of a set of TCT sub-arrays; 3) flexible control for the maximum power generation using BCC-DPP converters with model-based MPP voltage prediction. This is necessary since some TCT square arrays may still experience multiple power peaks due to the inequality of the solar irradiance within the rows in each sub-array group, even after applying MS-EC and IE methods. The robust control scheme of the proposed approach leads to a global MPP operation under various PSCs, unlike traditional MPPT methods that only search for one peak power point. Also, the optimal design of the BCCs and IBCs parasitic elements has shown fast and stable transient responses, as demonstrated in the experimental validation of the model. The performance of the combined scheme was evaluated by simulation studies under non-uniform shading patterns and compared favourably to the other existing reconfiguration techniques, such as MS-EC, IE and the conventional TCT array structure with only bypass diodes. Output power improvements of 11-48% and average efficiency of 98.95% have been achieved.

Appendix

A1. Coefficients of transfer functions in Section 3.1 are expressed as:

$$\alpha_3 = CC_nL, \quad \alpha_2 = \frac{C_nL}{R_{pv2}} + CL(1-K)\left(\frac{(1-K)}{R_{pv1}} - \frac{K}{R_{pv2}}\right)$$

$$\alpha_1 = C_n + CK + \frac{L(1-K)}{R_{pv2}}\left(\frac{(1-K)}{R_{pv1}} - \frac{K}{R_{pv2}}\right), \quad \alpha_0 = \frac{(1-K)^2}{R_{pv1}} + \frac{K^2}{R_{pv2}} \quad (\text{A.1})$$

$$\beta_5 = (CL)^2C_n, \quad \beta_4 = CC_nL^2\left(\frac{1}{R_{pv1}} + \frac{1}{R_{pv2}}\right)$$

$$\beta_3 = C_nL\left(2C + \frac{L}{R_{pv1}R_{pv2}}\right)$$

$$\beta_2 = L(C_n + CK^2 + C(LK)^2)\left(\frac{1}{R_{pv1}} + \frac{1}{R_{pv2}}\right)$$

$$\beta_1 = C_n + (K^2 + (1-K)^2)\left(C + \frac{L}{R_{pv1}R_{pv2}}\right), \quad \beta_0 = \frac{(1-K)^2}{R_{pv1}} + \frac{K^2}{R_{pv2}} \quad (\text{A.2})$$

$$\Omega_3 = CC_nL, \quad \Omega_2 = \frac{C_nL}{R_{pv1}} + CLK\left(\frac{K}{R_{pv2}} - \frac{(1-K)}{R_{pv1}}\right)$$

$$\Omega_1 = C_n + C(1-K) + \frac{LK}{R_{pv1}}\left(\frac{K}{R_{pv2}} - \frac{(1-K)}{R_{pv1}}\right), \quad \Omega_0 = \frac{(1-K)^2}{R_{pv1}} + \frac{K^2}{R_{pv2}} \quad (\text{A.3})$$

A2. Design of the parameters of a practical Bidirectional Cuk Converter (BCC) in Sub-section 3.1.1:

The capacitors $C_1 = C_2 = C$ are obtained from the output voltage ripple of the BCC, expressed as:

$$\Delta v_o = \frac{\Delta q_o}{C} = \frac{\Delta i_L}{8CF_s} \quad (\text{A. 4})$$

where, Δq_o is the surplus charge accumulated in capacitor C during the charging state. The output inductors $L_1 = L_2 = L$ are calculated based on the inductor current ripple during the switching off period, written as:

$$\Delta i_L = \frac{(1 - K_{11})V_o}{LF_s} \quad (\text{A. 5})$$

$$\Delta v_o = \frac{(1 - K_{11})}{8CLF_s^2} V_o = \frac{\pi^2(1 - K_{11})}{2} \left(\frac{F_c}{F_s}\right)^2 V_o \quad (\text{A. 6})$$

The output voltage ripple Δv_o can be reduced by choosing low-pass filter parameters such that $F_s \gg F_c$. L and C dictate appropriate F_c ; hence these components values may be pre-determined based on the compromise between the ripple requirements and physical converter size.

References

1. Prince Winston, D., et al., *Parallel power extraction technique for maximizing the output of solar PV array*. Solar Energy, 2021. **213**: p. 102-117.
2. Zhang, X., et al., *Optimal mileage-based PV array reconfiguration using swarm reinforcement learning*. Energy Conversion and Management, 2021. **232**: p. 113892.
3. Ajmal, A.M., et al., *Static and dynamic reconfiguration approaches for mitigation of partial shading influence in photovoltaic arrays*. Sustainable Energy Technologies and Assessments, 2020. **40**: p. 100738.
4. Dhanalakshmi, B. and N. Rajasekar, *A novel Competence Square based PV array reconfiguration technique for solar PV maximum power extraction*. Energy Conversion and Management, 2018. **174**: p. 897-912.
5. Venkateswari, R. and N. Rajasekar, *Power enhancement of PV system via physical array reconfiguration based Lo Shu technique*. Energy Conversion and Management, 2020. **215**: p. 112885.
6. Manjunath, H.N. Suresh, and S. Rajanna, *Performance enhancement of Hybrid interconnected Solar Photovoltaic array using shade dispersion Magic Square Puzzle Pattern technique under partial shading conditions*. Solar Energy, 2019. **194**: p. 602-617.
7. Agrawal, N., B. Bora, and A. Kapoor, *Experimental investigations of fault tolerance due to shading in photovoltaic modules with different interconnected solar cell networks*. Solar Energy, 2020. **211**: p. 1239-1254.
8. Manjunath, H.N. Suresh, and S. Rajanna, *Reduction of mislead power and mismatch power loss under partial shading conditions using novel square matrix shade dispersion technique*. Solar Energy, 2020. **207**: p. 1364-1383.
9. Meerimatha, G. and B.L. Rao, *Novel reconfiguration approach to reduce line losses of the photovoltaic array under various shading conditions*. Energy, 2020. **196**: p. 117120.
10. Tatabhatla, V.M.R., A. Agarwal, and T. Kanumuri, *Improved power generation by dispersing the uniform and non-uniform partial shades in solar photovoltaic array*. Energy Conversion and Management, 2019. **197**: p. 111825.

11. Satpathy, P.R. and R. Sharma, *Parametric indicators for partial shading and fault prediction in photovoltaic arrays with various interconnection topologies*. Energy Conversion and Management, 2020. **219**: p. 113018.
12. Lakshika, K.A.H., et al., *Reconfigurable solar photovoltaic systems: A review*. Heliyon, 2020. **6**(11): p. e05530.
13. Mehedi, I.M., et al., *Critical evaluation and review of partial shading mitigation methods for grid-connected PV system using hardware solutions: The module-level and array-level approaches*. Renewable and Sustainable Energy Reviews, 2021. **146**: p. 111138.
14. Muhammad Ajmal, A., et al., *Comparative analysis of two-step GA-based PV array reconfiguration technique and other reconfiguration techniques*. Energy Conversion and Management, 2021. **230**: p. 113806.
15. Rezk, H., A. Fathy, and M. Aly, *A robust photovoltaic array reconfiguration strategy based on coyote optimization algorithm for enhancing the extracted power under partial shadow condition*. Energy Reports, 2021. **7**: p. 109-124.
16. Sai Krishna, G. and T. Moger, *Reconfiguration strategies for reducing partial shading effects in photovoltaic arrays: State of the art*. Solar Energy, 2019. **182**: p. 429-452.
17. Sai Krishna, G. and T. Moger, *A novel adaptive dynamic photovoltaic reconfiguration system to mitigate mismatch effects*. Renewable and Sustainable Energy Reviews, 2021. **141**: p. 110754.
18. Yousri, D., D. Allam, and M.B. Eteiba, *Optimal photovoltaic array reconfiguration for alleviating the partial shading influence based on a modified harris hawks optimizer*. Energy Conversion and Management, 2020. **206**: p. 112470.
19. Mahmoud, Y. and E.F. El-Saadany, *Enhanced Reconfiguration Method for Reducing Mismatch Losses in PV Systems*. IEEE Journal of Photovoltaics, 2017. **7**(6): p. 1746-1754.
20. Malathy, S. and R. Ramaprabha, *Reconfiguration strategies to extract maximum power from photovoltaic array under partially shaded conditions*. Renewable and Sustainable Energy Reviews, 2018. **81**: p. 2922-2934.
21. La Manna, D., et al., *Reconfigurable electrical interconnection strategies for photovoltaic arrays: A review*. Renewable and Sustainable Energy Reviews, 2014. **33**: p. 412-426.
22. Sai Krishna, G. and T. Moger, *Improved SuDoKu reconfiguration technique for total-cross-tied PV array to enhance maximum power under partial shading conditions*. Renewable and Sustainable Energy Reviews, 2019. **109**: p. 333-348.
23. Sreekantha Reddy, S. and C. Yammani, *A novel Magic-Square puzzle based one-time PV reconfiguration technique to mitigate mismatch power loss under various partial shading conditions*. Optik, 2020. **222**: p. 165289.
24. Nasiruddin, I., et al., *Shade diffusion of partial shaded PV array by using odd-even structure*. Solar Energy, 2019. **181**: p. 519-529.
25. Sahu, H.S., S.K. Nayak, and S. Mishra, *Maximizing the Power Generation of a Partially Shaded PV Array*. IEEE Journal of Emerging and Selected Topics in Power Electronics, 2016. **4**(2): p. 626-637.
26. Etarhouni, M., B. Chong, and L. Zhang. *A PV Array Reconfiguration Algorithm for Minimising Partial Shading Effects*. in *2019 10th International Renewable Energy Congress (IREC)*. 2019.
27. Pendem, S.R., S. Mikkili, and P.K. Bonthagorla, *PV Distributed-MPP Tracking: Total-Cross-Tied Configuration of String-Integrated-Converters to Extract the Maximum Power Under Various PSCs*. IEEE Systems Journal, 2020. **14**(1): p. 1046-1057.

28. Jeong, H., et al., *Review of Differential Power Processing Converter Techniques for Photovoltaic Applications*. IEEE Transactions on Energy Conversion, 2019. **34**(1): p. 351-360.
29. Lee, H. and K. Kim, *Design Considerations for Parallel Differential Power Processing Converters in a Photovoltaic-Powered Wearable Application*. Energies, 2018. **11**: p. 3329.
30. Mao, M., et al., *MPPT using modified salp swarm algorithm for multiple bidirectional PV-Cuk converter system under partial shading and module mismatching*. Solar Energy, 2020. **209**: p. 334-349.
31. Chong, B.V.P. and L. Zhang, *Controller design for integrated PV-converter modules under partial shading conditions*. Solar Energy, 2013. **92**: p. 123-138.
32. Etarhouni, M, Chong, B and Zhang, L (2020) *Optimal Design of Series-Parallel Differential Power Processing Converters for Photovoltaic Array Energy Systems*. The 37th European Photovoltaic Solar Energy Conference and Exhibition, Lisbon. pp. 1181-1187. ISBN 3-936338-73-6.
33. Chin, V.J., Salam, Z., Ishaque, K., 2017. An Accurate and fast computational algorithm for the two-diode model of PV module based on a hybrid method. IEEE Trans. Ind. Electron. <https://doi.org/10.1109/TIE.2017.2682023>.
34. Chen, Y., Sun, Y., Meng, Z., 2018. An improved explicit double-diode model of solar cells: Fitness verification and parameter extraction. Energy Convers. Manag. 169, 345–358.
35. Mohamed, A.W., Hadi, A.A., Fattouh, A.M., Jambi, K.M., 2017. L-SHADE with semi-parameter adaptation hybrid with CMA-ES for solving CEC 2017 benchmark problems. Proc. IEEE Congr. Evol. Comput. (CEC) 145–152.
36. S. Kumar Patro and R. P. Saini, *Mathematical modeling framework of a PV model using novel differential evolution algorithm*, Solar Energy, 2020, vol. **211**, pp. 210-226.
37. Shaiek, Y., et al., *Comparison between conventional methods and GA approach for maximum power point tracking of shaded solar PV generators*. Solar Energy, 2013. **90**: p. 107-122.
38. Ishaque, K. and Z. Salam, *A Deterministic Particle Swarm Optimization Maximum Power Point Tracker for Photovoltaic System Under Partial Shading Condition*. IEEE Transactions on Industrial Electronics, 2013. **60**(8): p. 3195-3206.
39. Ram, J.P. and N. Rajasekar, *A Novel Flower Pollination Based Global Maximum Power Point Method for Solar Maximum Power Point Tracking*. IEEE Transactions on Power Electronics, 2017. **32**(11): p. 8486-8499.